

UC Irvine

UC Irvine Previously Published Works

Title

Cyclin B3 is a dominant fast-acting cyclin that drives rapid early embryonic mitoses.

Permalink

<https://escholarship.org/uc/item/7zq9g6rm>

Journal

Journal of Cell Biology, 223(11)

Authors

Lara-Gonzalez, Pablo

Variyar, Smriti

Moghareh, Shabnam

et al.

Publication Date

2024-11-04


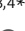



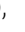


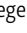



DOI

10.1083/jcb.202308034

Peer reviewed

REPORT

Cyclin B3 is a dominant fast-acting cyclin that drives rapid early embryonic mitoses

Pablo Lara-Gonzalez^{1,2} , Smriti Variyar^{3,4*} , Shabnam Moghareh^{1*} , Anh Cao Ngoc Nguyen^{1*} , Amrutha Kizhedathu¹ , Jacqueline Budrewicz² , Aleesa Schlientz^{3,4} , Neha Varshney^{3,4} , Andrew Bellaart^{3,4} , Karen Oegema^{2,3,4} , Lee Bardwell¹ , and Arshad Desai^{2,3,4} 

Mitosis in early embryos often proceeds at a rapid pace, but how this pace is achieved is not understood. Here, we show that cyclin B3 is the dominant driver of rapid embryonic mitoses in the *C. elegans* embryo. Cyclins B1 and B2 support slow mitosis (NEBD to anaphase ~600 s), but the presence of cyclin B3 dominantly drives the approximately threefold faster mitosis observed in wildtype. Multiple mitotic events are slowed down in cyclin B1 and B2-driven mitosis, and cyclin B3-associated Cdk1 H1 kinase activity is ~25-fold more active than cyclin B1-associated Cdk1. Addition of cyclin B1 to fast cyclin B3-only mitosis introduces an ~60-s delay between completion of chromosome alignment and anaphase onset; this delay, which is important for segregation fidelity, is dependent on inhibitory phosphorylation of the anaphase activator Cdc20. Thus, cyclin B3 dominance, coupled to a cyclin B1-dependent delay that acts via Cdc20 phosphorylation, sets the rapid pace and ensures mitotic fidelity in the early *C. elegans* embryo.

Introduction

During the division of cultured human somatic cells, the interval from nuclear envelope breakdown (NEBD) to sister chromatid separation/anaphase onset is ~30–60 min in the basal state when there are no stressors that prolong mitosis (Araujo et al., 2016). In these cells, the spindle assembly checkpoint is activated during each cell cycle and contributes to setting basal state mitotic timing (Meraldi et al., 2004). In contrast, during the rapid early embryonic divisions of species such as *Drosophila* and *Caenorhabditis elegans*, the basal NEBD-to-anaphase onset interval is ~3–5 min and the spindle checkpoint is only activated to delay mitotic progression when problems in chromosome-spindle attachment arise (Essex et al., 2009; Yuan and O’Farrell, 2015). How the accelerated mitotic pace characteristic of these early embryonic divisions is achieved is not clear.

Cyclin B–Cdk1 complexes orchestrate the execution of mitotic events (Crncec and Hochegger, 2019; Lindqvist et al., 2009). Following DNA replication, cyclin B gradually accumulates to drive a bi-stable Cdk1 activity switch (Hegarar et al., 2016; Hutter et al., 2017). Once active, cyclin B–Cdk1 complexes phosphorylate cellular substrates to direct chromosome condensation, NEBD,

spindle assembly, and chromosome segregation (Crncec and Hochegger, 2019; Lindqvist et al., 2009). In mid-mitosis, the anaphase-promoting complex/cyclosome (APC/C), an E3 ubiquitin ligase, targets cyclin B for degradation (Alfieri et al., 2017; Watson et al., 2019), leading to sister chromatid separation/anaphase onset and events associated with mitotic exit (Vagnarelli, 2021). In most metazoans, there are three cyclin B isoforms that activate Cdk1 in vitro: cyclins B1, B2, and B3 (Lozano et al., 2012). Of these, cyclin B1 and cyclin B2 are closely related in sequence and evolutionary origin, whereas cyclin B3 is divergent and shares sequence similarity to A-type cyclins (Gallant and Nigg, 1994; Lozano et al., 2012). Cyclin B3 plays important functions in the development of the germline and early embryos (Deyter et al., 2010; Jacobs et al., 1998; Nguyen et al., 2002; Yuan and O’Farrell, 2015). In vertebrates, cyclin B3 expression is largely germline specific and is essential for the transition from metaphase to anaphase of oocyte meiosis I (Bouftas et al., 2022; Karasu et al., 2019; Li et al., 2019; Zhang et al., 2015).

Here, we analyze the contributions of different cyclin B–Cdk1 complexes to rapid mitoses of the early *C. elegans* embryo, where

¹Department of Developmental and Cell Biology, University of California, Irvine, Irvine, CA, USA; ²Ludwig Institute for Cancer Research, La Jolla, CA, USA; ³Department of Cell and Developmental Biology, University of California, San Diego, San Diego, CA, USA; ⁴Department of Cellular and Molecular Medicine, University of California, San Diego, San Diego, CA, USA.

*S. Variyar, S. Moghareh, and A.C.N. Nguyen contributed equally to this paper. Correspondence to Pablo Lara-Gonzalez: plaragon@uci.edu; Arshad Desai: abdesai@ucsd.edu

J. Budrewicz’s current affiliations are Department of Molecular and Medical Genetics, Oregon Health & Science University, Portland, OR, USA, and Division of Reproductive and Developmental Sciences, Oregon National Primate Research Center, Beaverton, OR, USA.

© 2024 Lara-Gonzalez et al. This article is distributed under the terms of an Attribution–Noncommercial–Share Alike–No Mirror Sites license for the first six months after the publication date (see <http://www.rupress.org/terms/>). After six months it is available under a Creative Commons License (Attribution–Noncommercial–Share Alike 4.0 International license, as described at <https://creativecommons.org/licenses/by-nc-sa/4.0/>).

NEBD to anaphase onset takes only ~200 s. We show that, whereas embryos with cyclins B1 and B2 support slow mitosis (NEBD to anaphase ~600 s), the presence of cyclin B3 leads to a dominant approximately threefold acceleration in the pace of mitosis. Consistent with the *in vivo* phenotypic difference, cyclin B3-associated Cdk1 purified from embryos is significantly more active toward the model substrates H1 and Cdc20 than cyclin B1-associated Cdk1. In the context of rapid cyclin B3-driven mitoses, the additional presence of cyclin B1 introduces an ~1-min delay, dependent on Cdc20 phosphorylation, in APC/C activation and anaphase onset. Thus, in the early *C. elegans* embryo, the rapid pace of embryonic mitoses is achieved through the dominance of cyclin B3 in driving mitotic events, at least in part due to its ability to more potently activate Cdk1, coupled to introduction of a cyclin B1-dependent delay that ensures high fidelity of chromosome segregation by preventing premature anaphase onset.

Results and discussion

Cyclin B1 and cyclin B3 independently support Cdk1 activation during early embryonic divisions

To delineate the contributions of cyclin B isoforms (Fig. 1 A and Fig. S1 A) to early embryonic divisions in *C. elegans*, we employed RNA-mediated interference (RNAi) to compare the effects of their inhibition to knockdown of CDK-1. CDK-1 depletion prevented embryos from undergoing mitotic divisions and led to arrest at the one-cell stage with a large polyploid nucleus that arises due to continued DNA replication without intervening mitoses (Edgar and Orr-Weaver, 2001). CYB-3 can be specifically targeted by RNAi, but high sequence identity between CYB-1 and the two CYB-2 isoforms (CYB-2.1 and CYB-2.2, encoded by distinct genes) leads to their simultaneous targeting (referred to as *cyb-1&2(RNAi)*). Whereas simultaneous knockdown of all three cyclins (*cyb-1&2 + cyb-3(RNAi)*; No CYBs) led to an arrest similar to CDK-1 knockdown, expression of either CYB-1&2 or CYB-3 supported mitotic entry (Fig. 1, A–C; and Fig. S1 B). To evaluate the independent contributions of CYB-1 and CYB-2, we engineered a CYB-RECODE strain by introducing a single copy transgene expressing CYB-1, whose nucleotide sequence was altered to confer resistance to the double-stranded RNA (dsRNA) that targets endogenous CYB-1 and CYB-2 into a *cyb-1Δ* mutant background (Fig. 1 D and Fig. S1, B–E). The ability to selectively knock down CYB-1 versus CYB-2 in the CYB-RECODE strain was confirmed by immunoblotting (Fig. 1 E). Using this approach, we found that CYB-1, but not CYB-2, promoted entry into mitosis (Fig. 1 F and Fig. S2, A and B). These results indicate that CYB-1 and CYB-3 are independently capable of supporting CDK-1 activation during early embryonic divisions.

Cyclin B3 dominantly drives fast mitosis in early embryos

We next investigated the effect on mitosis of one-cell embryos of cyclin B isoform depletions. To complement prior surveys (Michael, 2016; van der Voet et al., 2009), we compared embryos expressing only CYB-1/2 to embryos expressing only CYB-3 in a strain with fluorescently labeled microtubules and chromosomes. This analysis revealed a striking difference: embryos in

which mitosis was driven by CYB-1/2 (*cyb-3(RNAi)*, hereafter referred to as “CYB-1/2-only”), took approximately three times longer to complete mitosis than embryos in which mitosis was driven by CYB-3 (*cyb-1/2(RNAi)*, hereafter referred to as “CYB-3-only”; Fig. 2, A and B). Monitoring spindle assembly revealed that CYB-1/2-only embryos had weaker microtubule density compared with control and CYB-3-only embryos (Fig. 2 C and Fig. S2 C; Deyter et al., 2010). Moreover, analysis of chromosome alignment kinetics (Cheerambathur et al., 2017) revealed that chromosome congression occurred at a similar rate in control and CYB-3-only embryos but was substantially slower in CYB-1/2-only embryos (Fig. 2, D and E). Thus, the overall pace of mitotic events including spindle assembly, chromosome alignment, and anaphase onset is substantially slower in CYB-1/2-only embryos compared with control and CYB-3-only embryos. When CYB-3 is present, it overrides the rate set by CYB-1/2 to dominantly drive an approximately threefold faster mitotic pace.

One explanation for the dominance of CYB-3 is that it represents the predominant cyclin B isoform during early embryonic divisions. However, quantification of the total embryo fluorescence at NEBD of *in situ* mNeogreen (mNG)-tagged CYB-1 and CYB-3 (Lara-Gonzalez et al., 2019) (Fig. S2, D and E) revealed equivalent levels of CYB-1 and CYB-3 in the early embryo (Fig. 2, F and G). Time-lapse imaging of the mNG fusions additionally revealed that CYB-3 is degraded after CYB-1 (Fig. 2 H and Fig. S2, D and E), in agreement with prior analysis of cyclin B3 in other systems (Nguyen et al., 2002; Sigrist et al., 1995).

Slow progression of cyclin B1- and B2-driven mitosis is not explained by delayed APC/C activation

Cyclin B3 has been implicated in controlling APC/C activation in meiosis and mitotic contexts (Bouftas et al., 2022; Garrido et al., 2020; Karasu et al., 2019; Li et al., 2019). The APC/C is a major Cdk1 substrate and its phosphorylation releases an auto-inhibitory loop, thereby facilitating binding to its activator Cdc20 (Fujimitsu et al., 2016; Garrido et al., 2020; Qiao et al., 2016; Zhang et al., 2016).

To address if the slow mitotic progression in CYB-1&2-only mitosis is related to delayed APC/C activation, we pursued three different avenues. First, we tested if activation of the spindle assembly checkpoint, which surveils chromosome-spindle attachments to control APC/C activity (Lara-Gonzalez et al., 2021; McAinsh and Kops, 2023; Musacchio, 2015), contributed to the observed slow mitosis of CYB-1&2-only embryos. The spindle assembly checkpoint does not control basal mitotic timing in early *C. elegans* embryos (Houston et al., 2023; Kim et al., 2017) but unattached kinetochores resulting from problems in spindle assembly activate the checkpoint and extend mitosis by inhibiting the APC/C (Essex et al., 2009). Codepletion of the checkpoint effector MAD-3 (Essex et al., 2009; Houston et al., 2023; Kim et al., 2017; Lara-Gonzalez et al., 2019) reduced the NEBD-anaphase onset interval in CYB-1/2-only embryos from ~630 to ~450 s (Fig. 3 A). However, checkpoint inactivation did not accelerate the rate of chromosome alignment (Fig. 3 B), and the overall mitotic duration remained ~2.5-fold longer than in controls (Fig. 3 C). Thus, the spindle assembly checkpoint is not

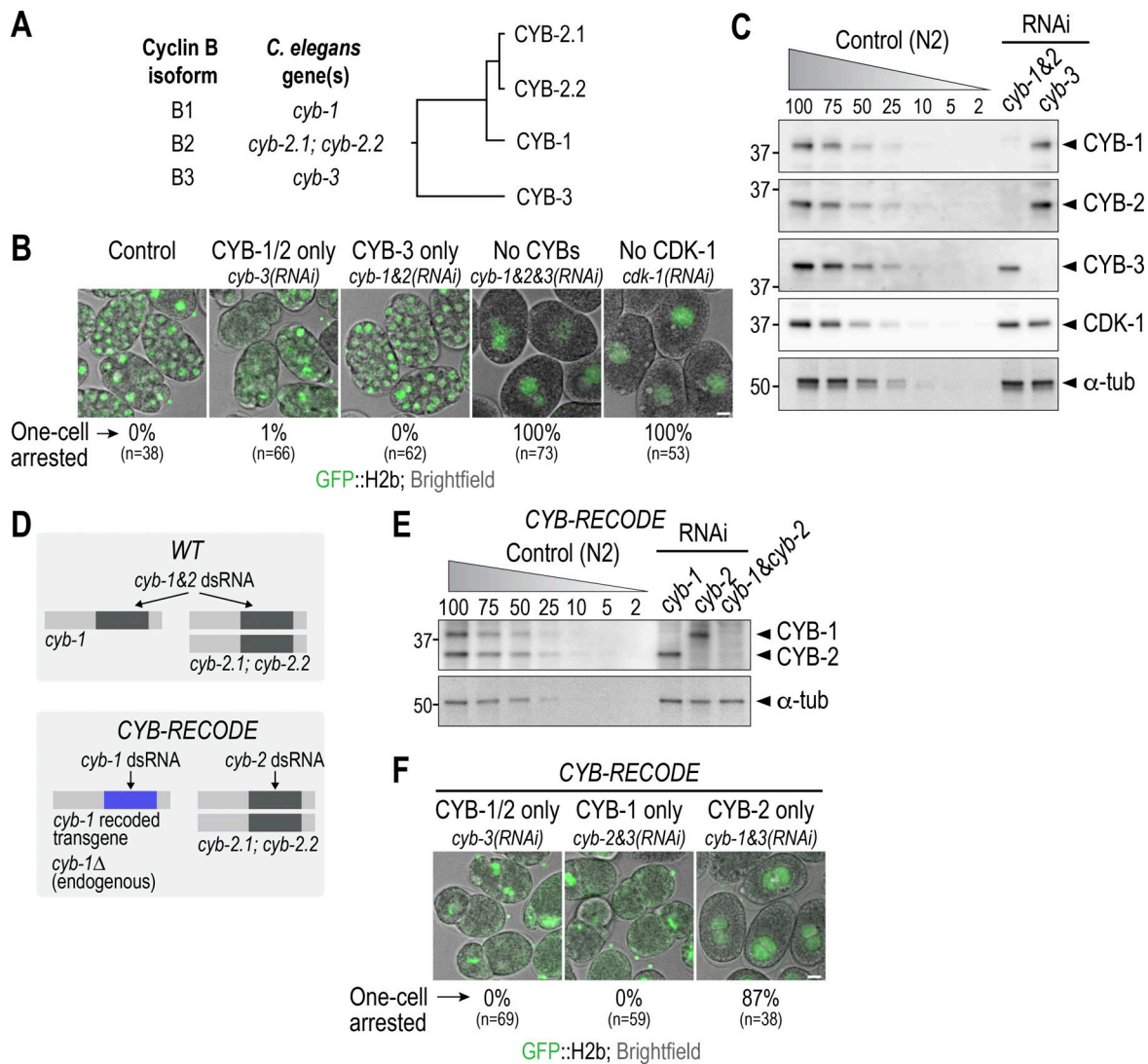


Figure 1. Cyclins B1 and B3 redundantly activate Cdk1 to promote embryonic divisions. (A) Phylogenetic tree showing gene names and relationship between *C. elegans* cyclin B isoforms. (B) Example images of embryos depleted for the specified proteins. To aid interpretation, the cyclin B(s) present are labeled on top and the RNAi condition employed to generate the specific cyclin B state on the bottom. Quantification of the percentage of interphase-arrested embryos with a single large nucleus is noted below each panel. (C) Immunoblot showing depletion of CYB-1&2 or CYB-3 by RNAi. A dilution curve of control (N2) worm extract was loaded to assess depletion efficiency; numbers above lanes indicate percent loading relative to RNAi samples. α -Tubulin serves as a loading control. (D) Schematic illustrating the principle behind the CYB-RECODE system for specific depletion of CYB-1 or CYB-2. (E) Validation of the CYB-RECODE system by immunoblotting, conducted as in panel C. α -Tubulin serves as a loading control. (F) Example images of CYB-RECODE embryos depleted for the specified proteins, as well as quantification of the percentage of interphase arrested embryos. Scale bars in B and F, 10 μ m; *n* is the total number of embryos scored per condition. Left numbers in C and E indicate the positions of the molecular weight marker in kDa. Source data are available for this figure: SourceData F1.

the primary reason why mitotic progression in CYB-1/2-only embryos is slow. In agreement with these findings, evaluation of APC/C activity by measuring the degradation of CYB-1::mNG in living embryos confirmed that APC/C activation is significantly delayed in CYB-1/2-only embryos compared with controls and that this delay is only modestly reduced by coinhibition of the checkpoint (Fig. 3, D and E; and Fig. S2 F).

Second, we considered the possibility that CYB-3 accelerates mitotic progression by counteracting inhibitory phosphorylation of Cdc20, which is known to hold APC/C activation in check by reducing Cdc20's affinity for the APC/C (Hein and Nilsson, 2016; Labit et al., 2012; Yudkovsky et al., 2000). Prior work in

the *C. elegans* embryo has shown that Cdk phosphorylation of a single conserved Cdk-targeted Threonine residue (T32) in the N-terminus of CDC-20 is important for proper mitotic timing (Houston et al., 2023; Kim et al., 2017). We found that the NEBD-to-anaphase interval was nearly identical in CYB-1/2-only embryos expressing wild-type (WT) or non-phosphorylatable T32A CDC-20 (Fig. S2 G). Thus, persistent CDC-20 phosphorylation does not explain the slow mitosis of CYB-1&2-only embryos.

Finally, we directly compared the phenotype of delaying APC/C activation to the phenotype of CYB-1&2-only embryos. For this purpose, we inhibited the APC/C using a temperature-sensitive allele of Apc4/EMB-30 (Furuta et al., 2000). At the

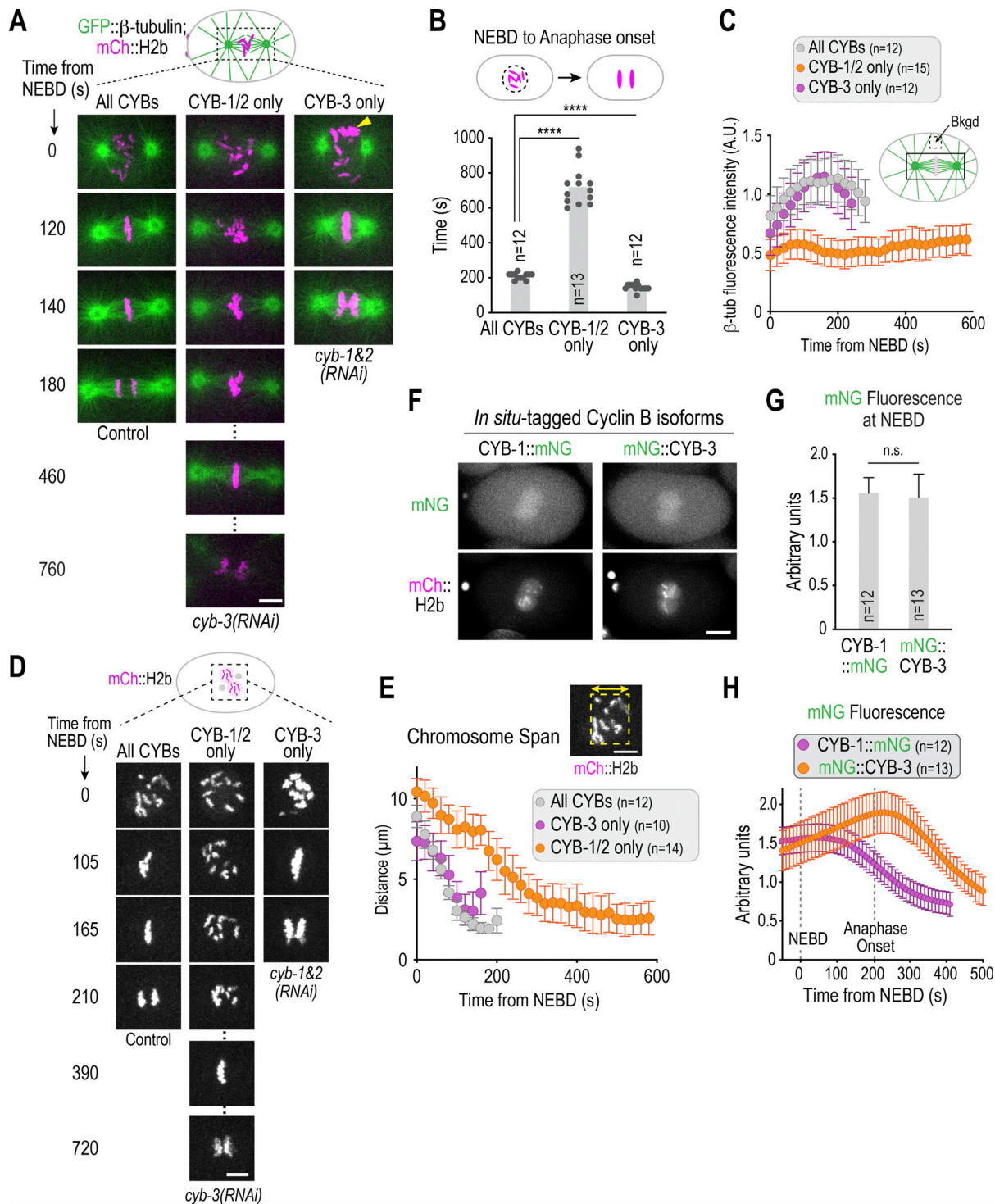


Figure 2. **CYB-1/2 supports slow mitosis, whereas CYB-3 dominantly drives rapid mitosis.** (A) Stills from time-lapse sequences of embryos expressing GFP-tagged β -tubulin and mCherry-tagged histone H2b for the specified conditions. To aid interpretation, the cyclin Bs present and supporting mitosis are labeled on top and the RNAi condition employed to generate the specific cyclin B state on the bottom. Yellow arrowhead indicates pronucleus with excess chromatin (see Fig. S2). (B) Quantification of the NEBD-to-anaphase interval for the specified conditions. Mean and individual embryo values are plotted. (C) Quantification of spindle β -tubulin intensity over time; background (Bkgd) fluorescence in a region adjacent to the spindle was subtracted, as indicated by the schematic. (D) Stills from time-lapse sequences of embryos expressing mCherry-tagged histone H2b for the indicated conditions. (E) Quantification of chromosome alignment kinetics by measurement of chromosome span for the indicated conditions. (F) Example images of embryos expressing endogenously tagged cyclin B isoforms. (G) Quantification of CYB-1::mNG and mNG::CYB-3 total embryo fluorescence intensity at NEBD. WT embryos lacking any mNG fusion were imaged under identical conditions to measure and subtract autofluorescence; see Fig. S2 E. (H) Quantification of embryo mNG fluorescence over time for the specified strains expressing *in situ*-tagged cyclin B isoforms (see also Fig. S2, D and E). In all graphs, *n* is the number of embryos analyzed and error bars are 95% confidence intervals. **** represents $P < 0.0001$ from Mann-Whitney tests; non-significant (n.s.) is $P > 0.05$. Scale bars, 5 μ m for panels A, D, and E; 10 μ m for panel F.

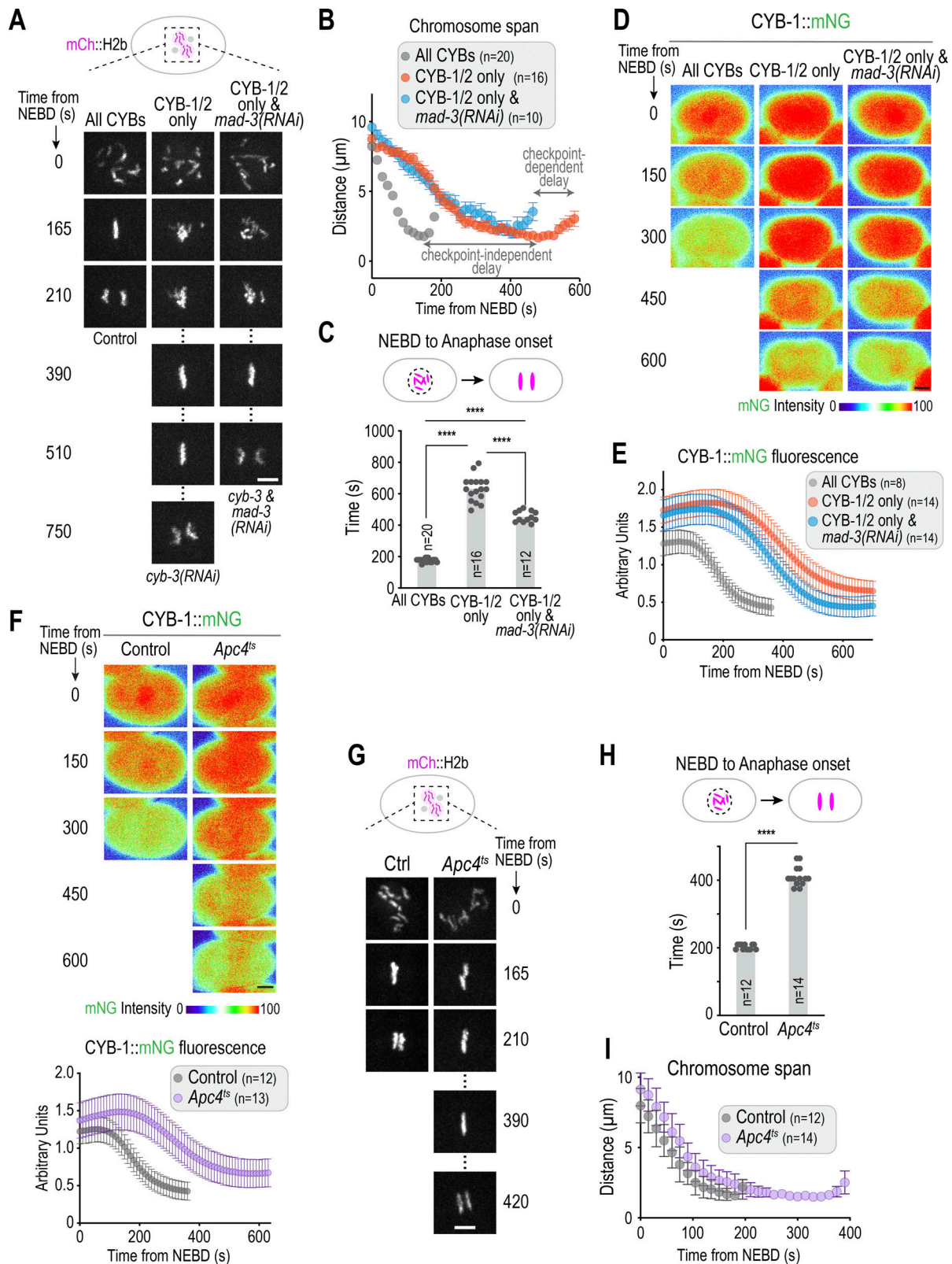


Figure 3. **Slow progression of CYB-1/2-driven early embryonic mitosis is not fully explained by delayed APC/C activation.** (A) Stills from time-lapse sequences of embryos expressing mCherry-tagged histone H2b for the specified conditions. (B) Quantification of the chromosome span (see Fig. 2, D and E) for the specified conditions. (C) Quantification of the NEBD-to-anaphase interval for the specified conditions. (D) Stills from time-lapse sequences of embryos expressing mNG-tagged CYB-1. The fluorescence intensity was pseudocolored to aid visualization (see also Fig. S2, D and E). (E) Quantification of CYB-1 fluorescence for the specified conditions. We note that CYB-1 levels were mildly elevated upon CYB-3 depletion, which may reflect either incomplete degradation in the preceding meiotic divisions or a compensatory mechanism caused by the reduction in total cyclin B levels. (F) Top: Stills from time-lapse

sequences of embryos expressing mNG-tagged CYB-1 and a temperature-sensitive mutant of the APC/C subunit *Apc4* (*emb-30(tn377)*; referred to herein as *Apc4^{ts}*). Fluorescence intensity was pseudocolored to aid visualization. Bottom: Quantification of CYB-1 fluorescence for the specified conditions. **(G)** Stills from time-lapse sequences for WT or *Apc4^{ts}* mutant embryos expressing mCherry-tagged histone H2b. **(H)** Quantification of the NEBD-to-anaphase time interval for the specified conditions. **(I)** Quantification of chromosome span over time for the specified conditions. In all graphs, *n* is the number of embryos analyzed and error bars, if shown, are the 95% confidence interval. **** represents $P < 0.0001$ from Mann-Whitney tests. Scale bars, 5 μm for A and G; 10 μm for D and F.

semi-permissive temperature of 20°C, *Apc4^{ts}* delayed CYB-1 degradation and caused a twofold increase in mitotic duration (Fig. 3, F–H; and Fig. S2 H), which is close to the ~2.5-fold increase observed in CYB-1/2-only embryos in which the checkpoint had been inactivated by MAD-3 depletion (Fig. 3 C). However, unlike in the MAD-3-depleted CYB-1/2-only embryos, chromosome alignment occurred with kinetics identical to controls in *Apc4^{ts}* embryos (Fig. 3 I). Collectively, these results indicate that CYB-3 dominantly accelerates the kinetics of APC/C activation, but directly delaying APC/C activation does not fully phenocopy the absence of CYB-3.

Cdk1 association is required for cyclin B3 to drive rapid embryonic mitosis

The above results suggest that CYB-3 sets the pace of mitosis in early embryos, likely by associating with CDK-1 to form active kinase complexes. To directly test the significance of CDK-1 association, we mutated key residues in CYB-3 that promote its interaction with CDK-1 (Y112A, I116A, and Y119A; referred to herein as CDK-1 binding mutant or CB^{Mut}; Fig. S3 A) (Brown et al., 2015; Goda et al., 2001). We confirmed loss of CDK-1 interaction in CYB-3 CB^{Mut} by immunoprecipitation from *C. elegans* extracts and coexpression in human cells (Fig. S3, B and C).

We next generated a replacement system for CYB-3 in which endogenous CYB-3 is depleted by RNAi and replaced by transgene-encoded untagged CYB-3 (Fig. S3 D). Transgene-encoded WT CYB-3 suppressed the penetrant lethality of *cyb-3(RNAi)* and rescued the significantly delayed chromosome alignment and anaphase onset in one-cell embryos (Fig. S3, E–G). By contrast, the CYB-3 CB^{Mut} mutant recapitulated the effects of CYB-3 depletion on mitotic timing, chromosome alignment, and embryonic viability observed following CYB-3 depletion (Fig. S3, F–J). These results establish that CYB-3 must associate with CDK-1 to drive rapid embryonic mitosis.

Cyclin B3 activates Cdk1 significantly more robustly than cyclin B1

The results above indicate that in the early *C. elegans* embryo CYB-3-driven mitosis is about three times faster than CYB-1/2-driven mitosis. One model for how CYB-3 supports rapid mitosis is that the enzymatic activity of CYB-3-CDK-1 is higher than that of CYB-1-CDK1; such a model has precedence in the analysis of different cyclin-CDK complexes in yeast and humans (Koivomagi et al., 2011; Loog and Morgan, 2005; Topacio et al., 2019).

To understand the basis for the difference between CYB-1/2-only and CYB-3-only mitosis, we analyzed CYB-1 and CYB-3-associated CDK-1 kinase activity. We engineered *C. elegans* strains, where the endogenous copy of either CYB-1 or CYB-3 was fused to a purification tag, and immunopurified each cyclin B isoform from embryo extracts (Fig. 4 A). While both CYB-1 and

CYB-3 associated with CDK-1, CYB-3 bound ~1.3 times the amount of CDK-1 compared with CYB-1 (Fig. 4, B and C). CDK-1 is regulated by both activating (pT179) and inhibitory (pY33) phosphorylation (Crncec and Hochegger, 2019), and we observed a similar ~1.3 increase in both pT179 and pY33 CDK-1 bound to CYB-3 compared with CYB-1 (Fig. S4 A). Mass spectrometric analysis of cyclin B isoform immunoprecipitates confirmed robust copurification of CDK-1 with CYB-1 and CYB-3 and no significant enrichment of other cyclin-dependent kinases (Fig. S4 B and Table S3).

We next compared the activities of CYB-1-CDK-1 versus CYB-3-CDK-1 complexes using equalized amounts of CDK-1 and histone H1 as a substrate. Under the assay conditions, CYB-3-CDK1 complexes exhibited ~25-fold higher activity toward histone H1 than CYB-1-CDK-1 (Fig. 4, D and E). Treatment with Cdk1 inhibitors (McCarthy Campbell et al., 2009; Potapova et al., 2006; Vassilev et al., 2006) suppressed this activity (Fig. S4 C). Thus, CYB-3 is a significantly more potent activator of CDK-1 H1 kinase activity than CYB-1.

If CYB-3 accelerates mitosis due to its greater potency as a CDK-1 activator relative to CYB-1, then elevating the amount of CYB-1 present may partially compensate for the absence of CYB-3. To test this prediction, we increased CYB-1 dosage using an integrated single-copy CYB-1 transgene. Increasing the dosage of CYB-1 partially but significantly suppressed the anaphase onset delay phenotype observed in CYB-1&2-only embryos (Fig. 4, F and G) and improved the overall quality of embryonic divisions (Fig. S4 D). However, the increased CYB-1 dosage did not significantly suppress the chromosome alignment defect (Fig. S4 E). To explore why CYB-3 is a more potent activator of CDK-1 than CYB-1, we generated strains expressing chimeras that swapped the divergent cyclin box domains of CYB-3 into CYB-1 (Fig. S4 F). Unfortunately, both chimeras were compromised in their ability to bind and activate CDK-1 relative to CYB-1 (Fig. S4, G and H), and thus were not investigated further. We conclude that CYB-3 activates CDK-1 significantly more potently than CYB-1 and that this property likely contributes to the ability of CYB-3 to dominantly drive rapid embryonic mitoses.

Cyclin B1 acts in the same pathway as Cdc20 phosphorylation to delay anaphase onset

One intriguing observation from the phenotypic analysis above is that the NEBD-to-anaphase onset interval in CYB-3-only embryos was ~60 s faster than in control embryos (Fig. 2 B). The chromosome span analysis indicated that chromosome alignment occurred with similar kinetics in control and CYB-3-only embryos, but the ~60-s delay between chromosome alignment and anaphase onset observed in the WT is absent in CYB-3-only embryos. To determine which cyclin(s) are responsible for this anaphase onset delay, we used the CYB-RECODE

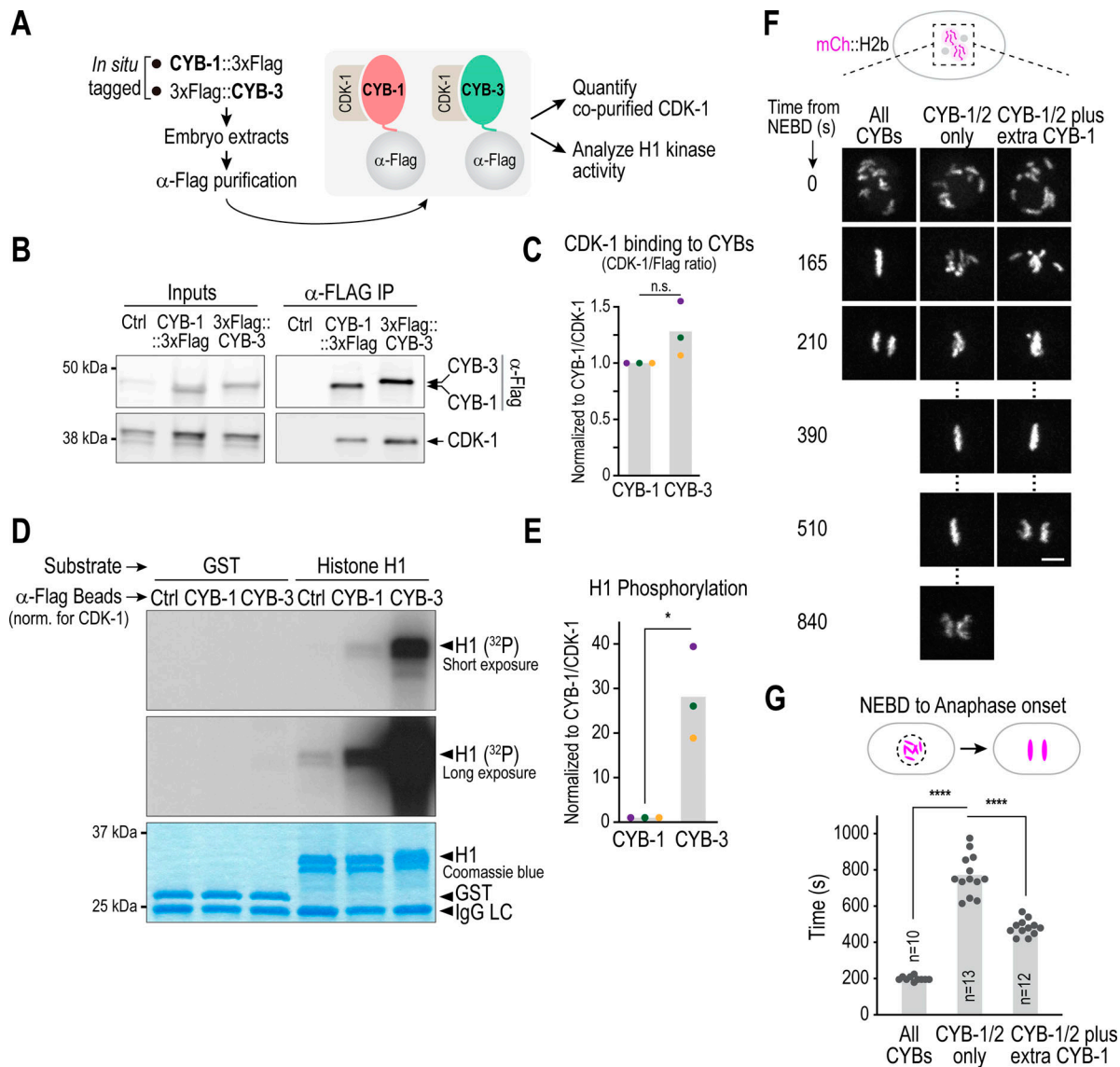


Figure 4. CYB-3 is a more potent activator of CDK-1 H1 kinase activity than CYB-1. (A) Schematic of experimental approach used to analyze CYB-1 and CYB-3 associated CDK-1 and histone H1 kinase activity. (B) Immunoblots showing input extracts and immunoprecipitates (IP) of Flag-tagged CYB-1 and CYB-3, as well as co-purified CDK-1. (C) Quantification of CDK-1 associated with each cyclin B isoform. The amount of CDK-1 co-purified with CYB-3 was normalized relative to the amount of CDK-1 co-purified with CYB-1 in each experiment. Colored dots represent three independent experiments; bar is the mean value. n.s. is not significant ($P > 0.05$) from an unpaired t test (data distribution was assumed to be normal although this was not formally tested). (D) Histone H1 kinase activity of bead-concentrated cyclin B isoforms. To compensate for the slightly higher level of CDK-1 present in the CYB-3 immunoprecipitates, the amount of CDK-1 present was equalized prior to performing the kinase assays. Both short and long exposures of the autoradiogram are shown. Coomassie gel shows the substrates; GST served as a control substrate. IgG LC corresponds to the light chain of Ig. (E) Quantification of H1 kinase activity in three independent experiments. The amount of H1 kinase activity co-purified with CYB-3 was normalized relative to the amount of H1 kinase activity co-purified with CYB-1 in each experiment. Colored dots represent three independent experiments; bar is the mean value. * represents $P = 0.0107$ from an unpaired t test (data distribution was assumed to be normal although this was not formally tested). (F) Stills from time-lapse sequences of embryos expressing mCherry-tagged histone H2b for the indicated conditions. “Extra CYB-1” refers to the presence of a single copy transgene expressing CYB-1. Scale bar, 5 μm . (G) Quantification of the NEBD to anaphase interval for the specified conditions. Mean and individual embryo values are plotted. n is the number of embryos analyzed and error bars are 95% confidence intervals. **** represents $P < 0.0001$ from a Mann-Whitney test (G). Left numbers in B and D represent the positions of the molecular weight marker in kDa. Source data are available for this figure: SourceData F4.

system to reintroduce CYB-1, CYB-2, or both (control) into CYB-3-only embryos (Fig. 5 A). The results indicate that reintroduction of CYB-1, but not CYB-2, in CYB-3-only embryos was sufficient to restore the ~60-s delay between chromosome alignment and anaphase onset observed in WT embryos (Fig. 5, A and B). As loss of the spindle assembly checkpoint does not

accelerate entry into anaphase in *C. elegans* embryos (Houston et al., 2023; Kim et al., 2017), we determined if CYB-1 delays anaphase onset by acting in the same pathway as inhibitory CDC-20 phosphorylation on T32 (Fig. 5 C). To test this possibility, we compared mitotic duration in CYB-3-only embryos expressing transgene-encoded WT or T32A CDC-20 in a *cdc-20* Δ background

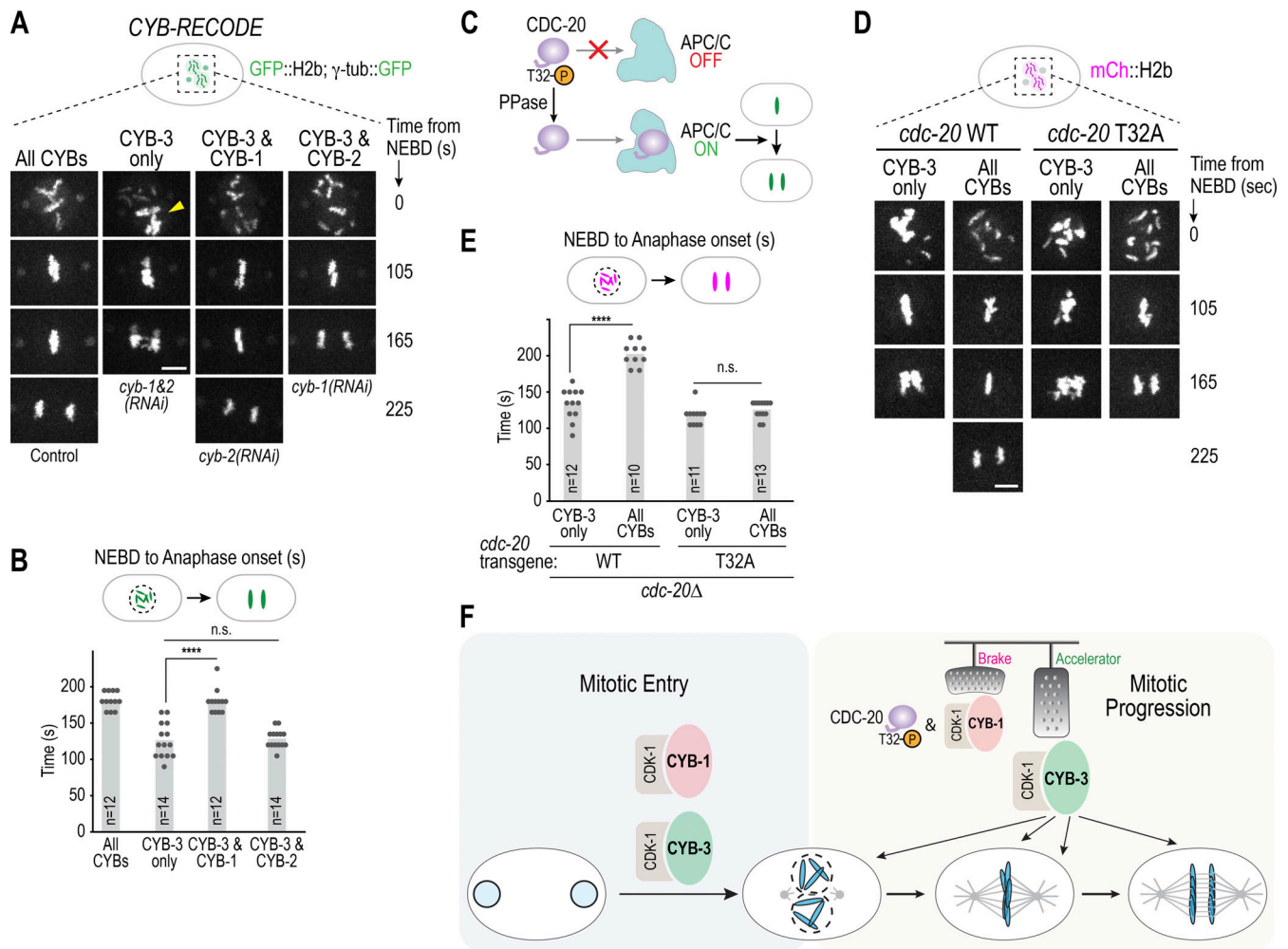


Figure 5. CYB-1 acts in the same pathway as CDC-20 phosphorylation to delay anaphase onset. (A) Stills from time-lapse sequences of CYB-RECODE embryos expressing GFP-tagged histone H2b and γ -tubulin, for the indicated conditions. Yellow arrowhead points to excess chromatin caused by meiotic defects (see Fig. S2, A and B). (B) Quantification of the NEBD-to-anaphase time interval for the specified conditions. (C) Schematic describing how phosphorylation (P) of CDC-20 at the Cdk-targeted Thr32 residue controls APC/C activation and anaphase onset. (D) Stills from time-lapse sequences of embryos expressing mCherry-tagged histone H2b and either WT or T32A CDC-20 in the background of a *cdc-20* null allele. *cyb-1/2(RNAi)* was used to generate the CYB-3-only condition. (E) Quantification of the NEBD-to-anaphase time interval for the specified conditions. The “All CYBs” conditions are the same as for Fig. S2 G. In all graphs, *n* represents the number of embryos analyzed. **** represents $P < 0.0001$ from Mann-Whitney tests; non-significant (n.s.) is $P > 0.05$. Scale bars in A and D are 5 μ m. (F) Model summarizing key findings of the work. Both CYB-3 and CYB-1 support mitotic entry but play strikingly different roles during mitosis, schematized by the accelerator and the brake pedals, respectively. CYB-3 robustly activates CDK-1 and is the dominant cyclin B driving rapid mitosis while CYB-1 delays anaphase onset, acting in the same pathway as CDC-20 phosphorylation, to ensure chromosome segregation fidelity.

(Fig. 5, D and E). If CYB-1 delays anaphase onset by acting in the same pathway as CDC-20 T32 phosphorylation, then CYB-1 should delay anaphase onset in the presence of WT but not T32A mutant CDC-20, which is in fact what we observed (Fig. 5, D and E). We conclude that CYB-1 and CDC-20 phosphorylation act in the same pathway to introduce a delay between chromosome alignment and anaphase onset. Using the purified N-terminal tail of CDC-20, which contains T32 as a substrate, we did not observe preferential phosphorylation by CYB-1-CDK-1 relative to CYB-3-CDK-1 (Fig. S4 I); instead, as with histone H1, we observed significantly greater phosphorylation by CYB-3-CDK-1. Thus, at present, the precise relationship between CYB-1-CDK-1 and CDC-20 T32 phosphorylation is unclear. Notably, abrogating the delay between alignment and anaphase onset reduces the robustness of chromosome segregation (Kim et al.,

2017), highlighting the functional significance of the CYB-1 and CDC-20 phosphorylation-dependent delay.

Conclusion

The results reported here highlight a division of labor between cyclin B1 and cyclin B3 in controlling rapid embryonic mitoses in *C. elegans*. Cyclin B3 is the dominant fast-acting cyclin that enables rapid early embryonic cell divisions by robustly activating Cdk1 to drive multiple mitotic processes, including activation of the APC/C. At the same time, cyclin B1 acts to ensure fidelity of chromosome segregation by introducing a delay between chromosome alignment and anaphase onset. Prior work in vertebrate oocytes has highlighted a critical function for cyclin B3 in promoting the metaphase-to-anaphase transition in oocyte meiosis I by targeting the APC/C inhibitor Emi2/XErp1 for

degradation (Bouftas et al., 2022; Karasu et al., 2019; Li et al., 2019). Cyclin B3 is not essential for anaphase of meiosis I in *C. elegans* oocytes (Fig. S2 A), likely due to the absence of an Emi2/Xerpl ortholog responsible for the metaphase II-stage oocyte arrest in vertebrates that is alleviated upon fertilization. *C. elegans* oocytes do not exhibit metaphase II arrest as their maturation and ovulation are directed by constitutive signals from sperm that are produced earlier in development and stored in the spermatheca (McCarter et al., 1999).

It is currently unclear why CYB-3 activates CDK-1 kinase activity directed toward histone H1 and the CDC-20 N-terminus significantly more potently than CYB-1. One potential explanation is the mechanism by which CYB-1 and CYB-3 direct CDK-1 activity toward substrates. Cyclin Bs contain two substrate recognition motifs: the hydrophobic patch and the basic patch (Loog and Morgan, 2005; Yu et al., 2021). While both of these substrate-binding motifs are present in CYB-1 and CYB-3, divergence in their sequence may contribute to differences between the cyclin B isoforms. An alternative possibility is that CYB-1 and CYB-3 differentially control the activity of CDK-1 by inducing different conformations of CDK-1's active site (Valk et al., 2023).

With respect to CYB-1 and CDC-20 phosphoregulation, while genetic analysis indicates their action in a common pathway, there is currently a lack of evidence for CYB-1-CDK-1 selectively phosphorylating CDC-20. Thus, an alternative possibility is that another kinase targets T32 and CYB-1-CDK-1 acts downstream, for instance, by protecting CDC-20 from dephosphorylation or limiting its interaction with the APC/C. Of note, in prior analysis, we found that CYB-1/2 works with CDC-20 phosphorylation to promote the G2-to-M transition in germ cell precursors (Lara-Gonzalez et al., 2019). Thus, CYB-1 and CDC-20 phosphorylation act in the same pathway in at least two distinct contexts. Aside from mitotic duration, CYB-1-CDK-1 also controls spindle length through an unknown mechanism (Fig. S2 C), highlighting additional specific roles. Collectively, the analysis here indicates that differences in the intrinsic ability to activate Cdk1 kinase as well as targeting of specific substrates underlies the division of labor between cyclin B isoforms to drive fast yet accurate early embryonic mitoses.

Materials and methods

C. elegans strains

The list of strains used in this study is in Table S1. *C. elegans* strains were maintained at 20°C in nematode growth media plates containing 50 µg/ml Streptomycin and seeded with the *Escherichia coli* OP50-1 strain. For generating transgenic lines, we used the Mos1 Single-Copy Insertion (MosSCI) method (Frøkjær-Jensen et al., 2008). Briefly, transgenes were cloned into either pCFJ352 or pCFJ151 vectors and injected into strains EG6701 or EG6699 to generate single-copy insertions in chromosome I or II, respectively (Frøkjær-Jensen et al., 2008). Transformants were selected based on their ability to rescue the *unc* mobility defect of the parental strains, and successful integrants were confirmed by PCR.

For the *cyb-1* and *cyb-3* RNAi replacement systems, we engineered constructs where a region of the coding sequence was

modified to introduce silent mutations to render them resistant to a dsRNA targeting the endogenous gene (Fig. S1 C and Fig. S3 D).

RNAi

dsRNAs were synthesized by in vitro transcription using PCR products containing sites for the T3 and T7 RNA polymerases as templates (Hattersley et al., 2018). Oligonucleotides used for dsRNA synthesis are listed in Table S2. dsRNAs were injected into the gut granules of L4 stage larvae at a final concentration of 0.8–1 mg/ml. Injected animals were recovered for 36–48 h at 20°C before imaging. For embryonic lethality assays, L4-stage worms injected with dsRNAs were recovered at 20°C for 24 h, singled onto 35-mm plates, and allowed to lay progeny for an additional 24 h before the mothers were removed. The next day, the total number of dead embryos and living larvae per plate was scored.

Antibody generation

For CYB-3 antibody production, rabbits were immunized with maltose-binding protein (MBP) fused to full-length CYB-3. Specific antibodies were affinity purified from the serum using a fragment containing amino acids 1–110 of CYB-3 fused to GST to prevent the purification of antibodies against MBP (Desai et al., 2003). Antibody specificity was validated by western blot against a lysate from worms treated with a dsRNA targeting endogenous CYB-3 (Fig. 1 C).

Because of the high amino acid sequence identity between CYB-1 and CYB-2, antibodies against these proteins were raised against their C-terminal end using the peptides CEKINRMGQNAKVDASEME and CRMGRNLEASEAETSEME, respectively. Note that the latter peptide sequence corresponds to CYB-2.2 but the antibody also detects CYB-2.1 due to their sequence similarity. Antibody specificity was confirmed by immunoblotting.

Immunoprecipitation of mNG-tagged CYB-3

C. elegans strains expressing mNG-tagged CYB-3 (WT or CB^{Mut}) were seeded onto 10-mm plates and grown for 4 days at 20°C when most of the population was adults. Animals were washed off the plates with M9 buffer (22 mM KH₂PO₄, 42 mM Na₂HPO₄, 86 mM NaCl, and 1 mM MgSO₄·7H₂O) and collected by centrifugation at 600 *g* for 3 min. After two rounds of washing, pellets were resuspended in 1.5 ml of lysis buffer (50 mM HEPES pH 7.4, 1 mM EDTA, 1 mM MgCl₂, 100 mM KCl, 10% glycerol, 0.1% Triton X-100, 1 mM DTT, cOmplete Protease Inhibitor Cocktail [Roche]). Lysates were generated by sonication and cleared by centrifugation at 20,000 *g* for 30 min at 4°C and incubated with mNG-nAb Agarose Beads (#ABP-nAb-MNGAK20; Allele Biotech) overnight at 4°C with rotation. Beads were washed four times with lysis buffer and eluted by resuspension in 2× sample buffer (116.7 mM Tris-HCl pH 6.8, 3.3% SDS, 200 mM DTT, 10% glycerol, bromophenol blue).

Immunoprecipitation of Flag-tagged CYBs

C. elegans strains expressing in situ-tagged CYB-1::3xFlag or 3xFlag::CYB-3, as well as N2 controls, were grown in liquid

media, and embryos were collected, flash-frozen with liquid nitrogen, and stored at -80°C (Zanin et al., 2011). Approximately 100 mg of frozen embryo pellet were resuspended with 500 μl of lysis buffer (50 mM HEPES pH 7.4, 1 mM EDTA, 1 mM MgCl_2 , 150 mM KCl, 10% glycerol, 0.1% Triton X-100, 1 mM DTT, cOmplete protease inhibitor cocktail [Sigma-Aldrich]) and lysed by sonication. Extracts were cleared by two rounds of centrifugation at 20,000 g for 30 min at 4°C and incubated with 50 μl of anti-Flag M2 magnetic beads (#M8823-1ML; Sigma-Aldrich), overnight at 4°C in an end-over-end rotator. Beads were then washed four times with 1 ml of lysis buffer and 0.25 of the total bead volume was transferred to a different tube and re-suspended in 2 \times sample buffer (116.7 mM Tris-HCl pH 6.8, 3.3% SDS, 200 mM DTT, 10% glycerol, bromophenol blue) for immunoblotting analysis.

Expression and purification of proteins in FreeStyle 293-F cells

Myc-tagged CYB-3 (WT or CB^{Mut}) and FLAG-tagged CDK-1 constructs were expressed in FreeStyle 293-F cells (Thermo Fisher Scientific) (Ohta et al., 2021). Cells were transfected using FreeStyle MAX Reagent and OptiPRO serum-free medium, according to the manufacturer's guidelines (Thermo Fisher Scientific). 20 ml of cells at a concentration of 10^6 cells/ml were transfected with 25 μg of DNA constructs. FreeStyle 293-F cells were incubated for 48 h at 37°C and 8% CO_2 on an orbital shaker platform rotating at 125 rpm. 10 ml of each sample was harvested and washed with Dulbecco's phosphate buffer saline (ThermoFisher Scientific). Cells were then resuspended in 1 ml of lysis buffer (20 mM Tris/HCl pH 7.5, 150 mM NaCl, 1% Triton X-100, 5 mM EGTA, 1 mM DTT, 2 mM MgCl_2 , and one EDTA-free protease inhibitor cocktail tablet; Roche) and sonicated in an ice bath for 6 min. Samples were centrifuged at 13,000 rpm for 15 min at 4°C . For input samples, 50 μl of supernatant was added to 25 μl of 4 \times Laemmli sample buffer. The remaining 950 μl of lysate supernatant was incubated with anti-FLAG M2 magnetic beads (#M8823-1ML; Sigma-Aldrich) for 2 h at 4°C . The beads were washed five times with lysis buffer and resuspended in 60 μl of 4 \times Laemmli sample buffer.

Preparation of *C. elegans* extracts for immunoblotting

Between 40 and 60 adult worms per condition were transferred to tubes containing M9 buffer (22 mM KH_2PO_4 , 42 mM Na_2HPO_4 , 86 mM NaCl, and 1 mM $\text{MgSO}_4 \cdot 7\text{H}_2\text{O}$), washed four times with M9 containing 0.1% Tween-20, and then resuspended in 2 \times sample buffer (116.7 mM Tris-HCl pH 6.8, 3.3% SDS, 200 mM DTT, 10% glycerol, bromophenol blue). Extracts were then lysed by sonication followed by boiling.

Immunoblotting

The equivalent of 8–10 worms was loaded onto 4–12% NuPAGE Bis-Tris Gels (Invitrogen). Proteins were then transferred to nitrocellulose membranes, probed with primary antibodies, and detected using either horseradish (HRP)-conjugated secondary antibodies and WesternBright Sirius (Advansta) chemiluminescent substrate or alkaline phosphatase (AP)-conjugated secondary antibody and Western Blue Stabilized Substrate for Alkaline Phosphatase (Promega). Membranes were imaged

using a ChemiDoc MP imaging system (BioRad). For the experiments in Fig. 4 B and Fig. S4, A and G, fluorescent secondary antibodies were used, membranes were developed using a LI-COR imaging system, and protein bands were quantified using ImageJ.

For the experiment in Fig. S3 C, 4 μl of each pull-down sample was run on Mini-PROTEAN gels (Bio-Rad) and transferred to polyvinylidene difluoride membranes using the Trans-Blot Turbo Transfer System (Bio-Rad). Membranes were blocked with 5% nonfat dry milk in TBS-T (20 mM Tris, 150 mM NaCl, 0.1% Tween 20, pH 7.6) and incubated overnight with primary antibody solutions in 5% BSA in TBS-T, followed by incubation with peroxidase-conjugated anti-mouse IgG light chain antibodies (Jackson ImmunoResearch). Membranes were developed with SuperSignal West Femto substrates (Thermo Fisher Scientific) and imaged using a ChemiDoc MP system (Bio-Rad).

Antibodies used in this study were: rabbit anti-CYB-1, rabbit anti-CYB-2, rabbit anti-CYB-3 (all three generated in this study—see Antibody generation), rabbit anti-Cdk1 PSTAIRE (#06-923; EMD Millipore), mouse anti-Myc (clone 9E10, #M4439-100UL; Sigma-Aldrich), mouse anti- α -tubulin (clone DM1A, #T6199-200UL; Millipore), mouse anti-Actin (clone C4, #06-923; Millipore Sigma), mouse anti-Flag tag (clone M2, #F3165-.2MG; Sigma-Aldrich), rabbit anti-Cdk1 pY15 (equivalent to *C. elegans* pY33; #9111T; Cell Signaling Technology), and rabbit anti-Cdk1 pT161 (equivalent to *C. elegans* pT179; #9114S; Cell Signaling Technology). Secondary antibodies were: HRP-conjugated donkey anti-rabbit IgG (#711-035-152; Jackson ImmunoResearch), HRP-conjugated goat anti-mouse light chain (#115-035-174; Jackson ImmunoResearch), AP-conjugated goat anti-mouse IgG (#S3721; Promega), IRDye 800CW goat anti-rabbit IgG (#926-3221; LI-COR), and Alexa Fluor 680 goat anti-mouse IgG light chain specific (#115-625-174; Jackson ImmunoResearch).

Protein kinase reactions

The sequence corresponding to amino acids 1–160 of CDC-20 was cloned into a pET-21a-GST vector for expression in bacteria and purified using glutathione-Sepharose (Bardwell et al., 2022). Protein kinase reactions (20 μl) contained kinase assay buffer (50 mM Tris-HCl pH 7.5, 10 mM MgCl_2 , 0.1 mM EDTA, 2 mM DTT, 0.01% Brij 35), 0.5 μM substrate (GST, CDC-20^{1–160}::GST or histone H1; Sigma-Aldrich), 50 μM ATP, 1 μCi of [γ -³²P]ATP, and \sim 20 μl bed volume of bead-bound immunoprecipated Cdk/cyclin complex (or the control kinase-negative immunoprecipation). Reactions were incubated for 20 min at 30°C and then separated by 12% SDS-PAGE, visualized by exposure to an x-ray film, and quantified on an Amersham Typhoon phosphorimager.

Flavopiridol (#HY-10005; MedChemExpress) and RO-3306 (#HY-12529; MedChemExpress) were used as CDK-1 inhibitors. IC50s values were estimated at 0.5 and 5.0 μM of inhibitor concentration using the formula: $x(y - \text{min}) / (100 - y)$; where x is the concentration of drug, y is the kinase activity remaining at a specific drug concentration, and min is the remaining kinase activity under fully saturating drug concentrations. We assumed a value of $\text{min} = 16$ for our assays and averaged the IC50 values obtained with 0.5 and 5.0 μM of inhibitor concentration.

Mass spectrometry analysis

For mass spectrometry analysis, gravid adult worms either control (N2) or expressing in situ-tagged CYB-1::mNG::3xFlag or 3xFlag::CYB-3 were grown in liquid culture (Zanin et al., 2011), and 500 mg of sample was lysed by sonication in lysis buffer (50 mM HEPES pH 7.4, 1 mM EDTA, 1 mM MgCl₂, 100 mM KCl, 10% glycerol, 0.1% Triton X-100, 1 mM DTT, cOmplete protease inhibitor cocktail [Sigma-Aldrich]). Lysates were cleared by ultracentrifugation and immunoprecipitated using 50 µl of anti-Flag M2 agarose beads (#A2220-1ML; Sigma-Aldrich) overnight at 4°C. Beads were washed 3× with lysis buffer and 3× with PBS before processing for mass spectrometry analysis (Biomolecular and Proteomics Mass Spectrometry Facility, University of California, San Diego).

To discriminate between specific interactors and likely contaminants, proteins identified in the control pull-down sample were first removed from the CYB-1 and CYB-3 samples and then all interactors with less than two unique peptides were excluded. This analysis resulted in a list of 138 proteins for CYB-1 and 113 proteins for CYB-3. We highlighted high-confidence interactors as proteins with sequence coverage of >5% (Fig. S4 B). The list of unique and shared hits for CYB-1 and CYB-3 is reported in Table S3. The raw mass spectrometry proteomics data have been deposited to the ProteomeXchange Consortium via the PRIDE (Perez-Riverol et al., 2022) partner repository with the dataset identifier PXD053811 (PLG_01: N2 pull-down; PLG_02: CYB-1 pull-down; PLG_03: CYB-3 pull-down).

Fluorescence imaging of *C. elegans* embryos

C. elegans embryos were dissected from adults in M9 media and mounted onto 2% agarose pads, covered with a coverslip, and imaged at 20°C. Time-lapse imaging of one-cell embryos expressing CYB-1::mNG or mNG::CYB-3 was performed on a widefield deconvolution microscope (DeltaVision Elite; Applied Precision), run with a softWoRx program, and equipped with a charge-coupled device camera (pco.edge 5.5 sCMOS; PCO) and a 40× 1.35NA Uapo/340 objective (Olympus). Single stacks were acquired at 10-s intervals with 2% illumination intensity (on an InsightSSI illuminator) and 100-ms exposure for mNG and 10% illumination intensity and 100-ms exposure for mCherry.

Time-lapse imaging of embryos and oocytes expressing GFP::tubulin and mCherry::H2b was performed on an Andor Revolution XD Confocal System (Andor Technology), run with an Andor iQ3 software, and coupled with a spinning disk confocal scanner unit (CSU-10; Yokogawa) mounted on an inverted microscope (TE2000-E; Nikon), 60× 1.4 NA Plan Apochromat lenses, and outfitted with an electron multiplication back-thinned charged-coupled device camera (iXon; Andor Technology). For embryos, 5 × 2 µm stacks were taken every 15–20 s. Oocytes were imaged ex utero by cutting open adult worms on an 18 × 18-mm coverslip in 4 µl of egg buffer (118 mM NaCl, 48 mM KCl, 2 mM CaCl₂, 2 mM MgCl₂, and 0.025 mM of HEPES, filter sterilized before HEPES addition) and directly mounting on a pad of 2% agarose in egg buffer. Oocytes were imaged in a 13 × 1 µm stack every 20 s. Polar body extrusion success was evaluated based on the apparent return of extruded chromosomes to the cytoplasm before the end of imaging (after meiosis II).

Imaging analysis

For time-lapse experiments, NEBD was scored as the frame where free histone signal in the nucleus equilibrated with the cytoplasm, which was just before abrupt chromosome movements were evident. When imaging strains expressing fluorescently labeled tubulin, NEBD was scored as the first time frame where the signal from the microtubules invaded the nuclear region. Anaphase onset was scored as the first frame with visible separation of sister chromatids.

For the measurement of chromosome span, embryo images were first oriented in the anterior–posterior axis. Signals from the histone H2b channel were converted to binary and a bounding box was fitted to measure its width over time (Fig. 2 E). For quantification of tubulin signal intensities, a box was drawn around the spindle area, as depicted in Fig. 2 C. A smaller box was drawn in a region outside the spindle area to measure background fluorescence and the difference in average signal intensities between the two boxes was measured.

To quantify CYB-1::mNG and mNG::CYB-3 signal intensities over time, an area was drawn surrounding the whole embryo, and the integrated density was measured; background was subtracted by copying the same area to a region without any embryos. To correct for embryo autofluorescence, we calculated baseline autofluorescence levels in a strain that expressed mCherry-tagged histone H2b and no green fluorophore; the average autofluorescence levels were subtracted for all measurements (Fig. S2 E).

Statistical analyses

Statistical analysis was performed using Prism (Graphpad). In figures, asterisks denote statistical significance as calculated by Mann–Whitney tests (*, $P < 0.05$; **, $P < 0.01$; ***, $P < 0.001$; ****, $P < 0.0001$). For Fig. 4, C and E, statistical significance was calculated by *t* tests (*, $P < 0.05$).

Online supplemental material

Fig. S1 shows the validation of the CYB-RECODE system. Fig. S2 shows cyclin B phenotypes in meiosis and spindle elongation and analysis of cyclin B degradation kinetics in mitosis. Fig. S3 shows cyclin B3 accelerates mitotic events by activating CDK-1. Fig. S4 shows the biochemical characterization of cyclin B isoforms and analysis of chimeric versions. Table S1 lists the strains used in this study. Table S2 shows oligonucleotides used for dsRNA production. Table S3 shows mass spectrometry analysis of CYB-1 and CYB-3 interactors.

Data availability

Data are available in the primary article and the supplementary materials. Raw mass spectrometry data are available via ProteomeXchange with the identifier PXD053811. Original data, *C. elegans* strains, and plasmids generated in this study are available upon request from the corresponding authors.

Acknowledgments

We thank the Caenorhabditis Genetics Center, which is funded by National Institutes of Health (NIH) Office of Research

Infrastructure Programs (P40 OD010440), for providing strains and Majid Ghassemian at the University of California, San Diego Biomolecular and Proteomics Mass Spectrometry Facility for conducting the mass spectrometric analysis (NIH shared instrumentation grant number S10 OD021724).

This work was supported by grants from the NIH to P. Lara-Gonzalez (GM150786), A. Desai (GM074215), and K. Oegema (GM147265). A. Schlienz is supported by an NIH fellowship (F32GM145068). A. Desai and K. Oegema acknowledge salary support from the Ludwig Institute for Cancer Research.

Author contributions: P. Lara-Gonzalez: Conceptualization, Data curation, Formal analysis, Funding acquisition, Investigation, Methodology, Project administration, Supervision, Validation, Visualization, Writing—original draft, S. Variyar: Formal analysis, Investigation, S. Moghareh: Conceptualization, Formal analysis, Investigation, Methodology, Visualization, A.C.N. Nguyen: Conceptualization, Investigation, Methodology, Visualization, A. Kizhedathu: Conceptualization, Formal analysis, Investigation, Methodology, Visualization, J. Budrewicz: Investigation, A. Schlienz: Investigation, Writing—review & editing, N. Varshney: Investigation, A. Bellaart: Investigation, K. Oegema: Supervision, Writing—review & editing, L. Bardwell: Investigation, A. Desai: Conceptualization, Funding acquisition, Project administration, Resources, Supervision, Visualization, Writing—original draft, Writing—review & editing.

Disclosures: The authors declare no competing interests exist.

Submitted: 3 August 2023

Revised: 27 April 2024

Accepted: 18 July 2024

References

- Alfieri, C., S. Zhang, and D. Barford. 2017. Visualizing the complex functions and mechanisms of the anaphase promoting complex/cyclosome (APC/C). *Open Biol.* 7:170204. <https://doi.org/10.1098/rsob.170204>
- Araujo, A.R., L. Gelens, R.S. Sheriff, and S.D. Santos. 2016. Positive feedback keeps duration of mitosis temporally insulated from upstream cell-cycle events. *Mol. Cell.* 64:362–375. <https://doi.org/10.1016/j.molcel.2016.09.018>
- Bardwell, A.J., B. Wu, K.Y. Sarin, M.L. Waterman, S.X. Atwood, and L. Bardwell. 2022. ERK2 MAP kinase regulates SUFU binding by multisite phosphorylation of GLI1. *Life Sci. Alliance.* 5:e202101353. <https://doi.org/10.26508/lsa.202101353>
- Bouftas, N., L. Schneider, M. Halder, R. Demmig, M. Baack, D. Cladière, M. Walter, H. Al Abdallah, C. Kleinhempel, R. Messaritaki, et al. 2022. Cyclin B3 implements timely vertebrate oocyte arrest for fertilization. *Dev. Cell.* 57:2305–2320.e6. <https://doi.org/10.1016/j.devcel.2022.09.005>
- Brown, N.R., S. Korolchuk, M.P. Martin, W.A. Stanley, R. Moukhametzianov, M.E.M. Noble, and J.A. Endicott. 2015. CDK1 structures reveal conserved and unique features of the essential cell cycle CDK. *Nat. Commun.* 6:6769. <https://doi.org/10.1038/ncomms7769>
- Cheerambathur, D.K., B. Prevo, N. Hattersley, L. Lewellyn, K.D. Corbett, K. Oegema, and A. Desai. 2017. Dephosphorylation of the Ndc80 tail stabilizes kinetochore-microtubule attachments via the ska complex. *Dev. Cell.* 41:424–437.e4. <https://doi.org/10.1016/j.devcel.2017.04.013>
- Cnccac, A., and H. Hochegger. 2019. Triggering mitosis. *FEBS Lett.* 593: 2868–2888. <https://doi.org/10.1002/1873-3468.13635>
- Desai, A., S. Rybina, T. Müller-Reichert, A. Shevchenko, A. Shevchenko, A. Hyman, and K. Oegema. 2003. KNL-1 directs assembly of the microtubule-binding interface of the kinetochore in *C. elegans*. *Genes Dev.* 17:2421–2435. <https://doi.org/10.1101/gad.1126303>
- Deyter, G.M., T. Furuta, Y. Kurasawa, and J.M. Schumacher. 2010. *Caenorhabditis elegans* cyclin B3 is required for multiple mitotic processes

- including alleviation of a spindle checkpoint-dependent block in anaphase chromosome segregation. *PLoS Genet.* 6:e1001218. <https://doi.org/10.1371/journal.pgen.1001218>
- Edgar, B.A., and T.L. Orr-Weaver. 2001. Endoreplication cell cycles: More for less. *Cell.* 105:297–306. [https://doi.org/10.1016/S0092-8674\(01\)00334-8](https://doi.org/10.1016/S0092-8674(01)00334-8)
- Essex, A., A. Dammermann, L. Lewellyn, K. Oegema, and A. Desai. 2009. Systematic analysis in *Caenorhabditis elegans* reveals that the spindle checkpoint is composed of two largely independent branches. *Mol. Biol. Cell.* 20:1252–1267. <https://doi.org/10.1091/mbc.e08-10-1047>
- Frøkjær-Jensen, C., M.W. Davis, C.E. Hopkins, B.J. Newman, J.M. Thummel, S.P. Olesen, M. Grunnet, and E.M. Jørgensen. 2008. Single-copy insertion of transgenes in *Caenorhabditis elegans*. *Nat. Genet.* 40:1375–1383. <https://doi.org/10.1038/ng.248>
- Fujimitsu, K., M. Grimaldi, and H. Yamano. 2016. Cyclin-dependent kinase 1-dependent activation of APC/C ubiquitin ligase. *Science.* 352:1121–1124. <https://doi.org/10.1126/science.1243925>
- Furuta, T., S. Tuck, J. Kirchner, B. Koch, R. Auty, R. Kitagawa, A.M. Rose, and D. Greenstein. 2000. EMB-30: An APC4 homologue required for metaphase-to-anaphase transitions during meiosis and mitosis in *Caenorhabditis elegans*. *Mol. Biol. Cell.* 11:1401–1419. <https://doi.org/10.1091/mbc.11.4.1401>
- Gallant, P., and E.A. Nigg. 1994. Identification of a novel vertebrate cyclin: Cyclin B3 shares properties with both A- and B-type cyclins. *EMBO J.* 13: 595–605. <https://doi.org/10.1002/j.1460-2075.1994.tb06297.x>
- Garrido, D., M. Bourouh, É. Bonneil, P. Thibault, A. Swan, and V. Archambault. 2020. Cyclin B3 activates the Anaphase-Promoting Complex/Cyclosome in meiosis and mitosis. *PLoS Genet.* 16:e1009184. <https://doi.org/10.1371/journal.pgen.1009184>
- Goda, T., M. Funakoshi, H. Suhara, T. Nishimoto, and H. Kobayashi. 2001. The N-terminal helix of *Xenopus* cyclins A and B contributes to binding specificity of the cyclin-CDK complex. *J. Biol. Chem.* 276:15415–15422. <https://doi.org/10.1074/jbc.M011101200>
- Hattersley, N., P. Lara-Gonzalez, D. Cheerambathur, J.S. Gomez-Cavazos, T. Kim, B. Prevo, R. Khaliullin, K.Y. Lee, M. Ohta, R. Green, et al. 2018. Employing the one-cell *C. elegans* embryo to study cell division processes. *Methods Cell Biol.* 144:185–231. <https://doi.org/10.1016/bs.mcb.2018.03.008>
- Hégarat, N., S. Rata, and H. Hochegger. 2016. Bistability of mitotic entry and exit switches during open mitosis in mammalian cells. *BioEssays.* 38: 627–643. <https://doi.org/10.1002/bies.201600057>
- Hein, J.B., and J. Nilsson. 2016. Interphase APC/C-Cdc20 inhibition by cyclin A2-Cdk2 ensures efficient mitotic entry. *Nat. Commun.* 7:10975. <https://doi.org/10.1038/ncomms10975>
- Houston, J., M. Ohta, J.S. Gómez-Cavazos, A. Deep, K.D. Corbett, K. Oegema, P. Lara-Gonzalez, T. Kim, and A. Desai. 2023. BUB-1-bound PLK-1 directs CDC-20 kinetochore recruitment to ensure timely embryonic mitoses. *Curr. Biol.* 33:2291–2299.e10. <https://doi.org/10.1016/j.cub.2023.04.021>
- Hutter, L.H., S. Rata, H. Hochegger, and B. Novák. 2017. Interlinked bistable mechanisms generate robust mitotic transitions. *Cell Cycle.* 16:1885–1892. <https://doi.org/10.1080/15384101.2017.1371885>
- Jacobs, H.W., J.A. Knoblich, and C.F. Lehner. 1998. *Drosophila* Cyclin B3 is required for female fertility and is dispensable for mitosis like Cyclin B. *Genes Dev.* 12:3741–3751. <https://doi.org/10.1101/gad.12.23.3741>
- Karasu, M.E., N. Bouftas, S. Keeney, and K. Wassmann. 2019. Cyclin B3 promotes anaphase I onset in oocyte meiosis. *J. Cell Biol.* 218:1265–1281. <https://doi.org/10.1083/jcb.201808091>
- Kim, T., P. Lara-Gonzalez, B. Prevo, F. Meitinger, D.K. Cheerambathur, K. Oegema, and A. Desai. 2017. Kinetochores accelerate or delay APC/C activation by directing Cdc20 to opposing fates. *Genes Dev.* 31: 1089–1094. <https://doi.org/10.1101/gad.302067.117>
- Köivomägi, M., E. Valk, R. Venta, A. Iofik, M. Lepiku, D.O. Morgan, and M. Loog. 2011. Dynamics of Cdk1 substrate specificity during the cell cycle. *Mol. Cell.* 42:610–623. <https://doi.org/10.1016/j.molcel.2011.05.016>
- Labit, H., K. Fujimitsu, N.S. Bayin, T. Takaki, J. Gannon, and H. Yamano. 2012. Dephosphorylation of Cdc20 is required for its C-box-dependent activation of the APC/C. *EMBO J.* 31:3351–3362. <https://doi.org/10.1038/emboj.2012.168>
- Lara-Gonzalez, P., M.W. Moyle, J. Budrewicz, J. Mendoza-Lopez, K. Oegema, and A. Desai. 2019. The G2-to-M transition is ensured by a dual mechanism that protects cyclin B from degradation by Cdc20-activated APC/C. *Dev. Cell.* 51:313–325.e10. <https://doi.org/10.1016/j.devcel.2019.09.005>
- Lara-Gonzalez, P., J. Pines, and A. Desai. 2021. Spindle assembly checkpoint activation and silencing at kinetochores. *Semin. Cell Dev. Biol.* 117:86–98. <https://doi.org/10.1016/j.semcdb.2021.06.009>

- Li, Y., L. Wang, L. Zhang, Z. He, G. Feng, H. Sun, J. Wang, Z. Li, C. Liu, J. Han, et al. 2019. Cyclin B3 is required for metaphase to anaphase transition in oocyte meiosis I. *J. Cell Biol.* 218:1553–1563. <https://doi.org/10.1083/jcb.201808088>
- Lindqvist, A., V. Rodríguez-Bravo, and R.H. Medema. 2009. The decision to enter mitosis: Feedback and redundancy in the mitotic entry network. *J. Cell Biol.* 185:193–202. <https://doi.org/10.1083/jcb.200812045>
- Loog, M., and D.O. Morgan. 2005. Cyclin specificity in the phosphorylation of cyclin-dependent kinase substrates. *Nature.* 434:104–108. <https://doi.org/10.1038/nature03329>
- Lozano, J.C., V. Vergé, P. Schatt, J.L. Juengel, and G. Peaucellier. 2012. Evolution of cyclin B3 shows an abrupt three-fold size increase, due to the extension of a single exon in placental mammals, allowing for new protein-protein interactions. *Mol. Biol. Evol.* 29:3855–3871. <https://doi.org/10.1093/molbev/mss189>
- McAinsh, A.D., and G.J.P.L. Kops. 2023. Principles and dynamics of spindle assembly checkpoint signalling. *Nat. Rev. Mol. Cell Biol.* 24:543–559. <https://doi.org/10.1038/s41580-023-00593-z>
- McCarter, J., B. Bartlett, T. Dang, and T. Schedl. 1999. On the control of oocyte meiotic maturation and ovulation in *Caenorhabditis elegans*. *Dev. Biol.* 205:111–128. <https://doi.org/10.1006/dbio.1998.9109>
- McCarthy Campbell, E.K., A.D. Werts, and B. Goldstein. 2009. A cell cycle timer for asymmetric spindle positioning. *PLoS Biol.* 7:e1000088. <https://doi.org/10.1371/journal.pbio.1000088>
- Meraldi, P., V.M. Draviam, and P.K. Sorger. 2004. Timing and checkpoints in the regulation of mitotic progression. *Dev. Cell.* 7:45–60. <https://doi.org/10.1016/j.devcel.2004.06.006>
- Michael, W.M. 2016. Cyclin CYB-3 controls both S-phase and mitosis and is asymmetrically distributed in the early *C. elegans* embryo. *Development.* 143:3119–3127. <https://doi.org/10.1242/dev.141226>
- Musacchio, A. 2015. The molecular biology of spindle assembly checkpoint signaling dynamics. *Curr. Biol.* 25:R1002–R1018. <https://doi.org/10.1016/j.cub.2015.08.051>
- Nguyen, T.B., K. Manova, P. Capodici, C. Lindon, S. Bottega, X.Y. Wang, J. Refik-Rogers, J. Pines, D.J. Wolgemuth, and A. Koff. 2002. Characterization and expression of mammalian cyclin b3, a prepachytene meiotic cyclin. *J. Biol. Chem.* 277:41960–41969. <https://doi.org/10.1074/jbc.M203951200>
- Ohta, M., Z. Zhao, D. Wu, S. Wang, J.L. Harrison, J.S. Gómez-Cavazos, A. Desai, and K.F. Oegema. 2021. Polo-like kinase 1 independently controls microtubule-nucleating capacity and size of the centrosome. *J. Cell Biol.* 220:e202009083. <https://doi.org/10.1083/jcb.202009083>
- Perez-Riverol, Y., J. Bai, C. Bandla, D. García-Seisdedos, S. Hewapathirana, S. Kamatchinathan, D.J. Kundu, A. Prakash, A. Frericks-Zipper, M. Eisenacher, et al. 2022. The PRIDE database resources in 2022: A hub for mass spectrometry-based proteomics evidences. *Nucleic Acids Res.* 50:D543–D552. <https://doi.org/10.1093/nar/gkab1038>
- Potapova, T.A., J.R. Daum, B.D. Pittman, J.R. Hudson, T.N. Jones, D.L. Sattinover, P.T. Stukenberg, and G.J. Gorbisky. 2006. The reversibility of mitotic exit in vertebrate cells. *Nature.* 440:954–958. <https://doi.org/10.1038/nature04652>
- Qiao, R., F. Weissmann, M. Yamaguchi, N.G. Brown, R. VanderLinden, R. Imre, M.A. Jarvis, M.R. Brunner, I.F. Davidson, G. Litos, et al. 2016. Mechanism of APC/CCDC20 activation by mitotic phosphorylation. *Proc. Natl. Acad. Sci. USA.* 113:E2570–E2578. <https://doi.org/10.1073/pnas.1604929113>
- Sigrist, S., H. Jacobs, R. Stratmann, and C.F. Lehner. 1995. Exit from mitosis is regulated by *Drosophila* fizzy and the sequential destruction of cyclins A, B and B3. *EMBO J.* 14:4827–4838. <https://doi.org/10.1002/j.1460-2075.1995.tb00164.x>
- Topacio, B.R., E. Zatulovskiy, S. Cristea, S. Xie, C.S. Tambo, S.M. Rubin, J. Sage, M. Kõivomägi, and J.M. Skotheim. 2019. Cyclin D-Cdk4,6 drives cell-cycle progression via the retinoblastoma protein's C-terminal helix. *Mol. Cell.* 74:758–770.e4. <https://doi.org/10.1016/j.molcel.2019.03.020>
- Vagnarelli, P. 2021. Back to the new beginning: Mitotic exit in space and time. *Semin. Cell Dev. Biol.* 117:140–148. <https://doi.org/10.1016/j.semcdb.2021.03.010>
- Valk, E., M. Örd, I. Faustova, and M. Loog. 2023. CDK signaling via non-conventional CDK phosphorylation sites. *Mol. Biol. Cell.* 34:pe5. <https://doi.org/10.1091/mbc.E22-06-0196>
- van der Voet, M., M.A. Lorson, D.G. Srinivasan, K.L. Bennett, and S. van den Heuvel. 2009. *C. elegans* mitotic cyclins have distinct as well as overlapping functions in chromosome segregation. *Cell Cycle.* 8:4091–4102. <https://doi.org/10.4161/cc.8.24.10171>
- Vassilev, L.T., C. Tovar, S. Chen, D. Knezevic, X. Zhao, H. Sun, D.C. Heimbrook, and L. Chen. 2006. Selective small-molecule inhibitor reveals critical mitotic functions of human CDK1. *Proc. Natl. Acad. Sci. USA.* 103:10660–10665. <https://doi.org/10.1073/pnas.0600447103>
- Watson, E.R., N.G. Brown, J.M. Peters, H. Stark, and B.A. Schulman. 2019. Posing the APC/C E3 ubiquitin ligase to orchestrate cell division. *Trends Cell Biol.* 29:117–134. <https://doi.org/10.1016/j.tcb.2018.09.007>
- Yu, J., P. Raia, C.M. Ghent, T. Raisch, Y. Sadian, S. Cavadini, P.M. Sabale, D. Barford, S. Raunser, D.O. Morgan, and A. Boland. 2021. Structural basis of human separase regulation by securin and CDK1-cyclin B1. *Nature.* 596:138–142. <https://doi.org/10.1038/s41586-021-03764-0>
- Yuan, K., and P.H. O'Farrell. 2015. Cyclin B3 is a mitotic cyclin that promotes the metaphase-anaphase transition. *Curr. Biol.* 25:811–816. <https://doi.org/10.1016/j.cub.2015.01.053>
- Yudkovsky, Y., M. Shteinberg, T. Listovsky, M. Brandeis, and A. Hershko. 2000. Phosphorylation of Cdc20/fizzy negatively regulates the mammalian cyclosome/APC in the mitotic checkpoint. *Biochem. Biophys. Res. Commun.* 271:299–304. <https://doi.org/10.1006/bbrc.2000.2622>
- Zanin, E., J. Dumont, R. Gassmann, I. Cheeseman, P. Maddox, S. Bahmanyar, A. Carvalho, S. Niessen, J.R. Yates III, K. Oegema, and A. Desai. 2011. Affinity purification of protein complexes in *C. elegans*. *Methods Cell Biol.* 106:289–322. <https://doi.org/10.1016/B978-0-12-544172-8.00011-6>
- Zhang, S., L. Chang, C. Alfieri, Z. Zhang, J. Yang, S. Maslen, M. Skehel, and D. Barford. 2016. Molecular mechanism of APC/C activation by mitotic phosphorylation. *Nature.* 533:260–264. <https://doi.org/10.1038/nature17973>
- Zhang, T., S.T. Qi, L. Huang, X.S. Ma, Y.C. Ouyang, Y. Hou, W. Shen, H. Schatten, and Q.Y. Sun. 2015. Cyclin B3 controls anaphase onset independent of spindle assembly checkpoint in meiotic oocytes. *Cell Cycle.* 14:2648–2654. <https://doi.org/10.1080/15384101.2015.1064567>

Supplemental material

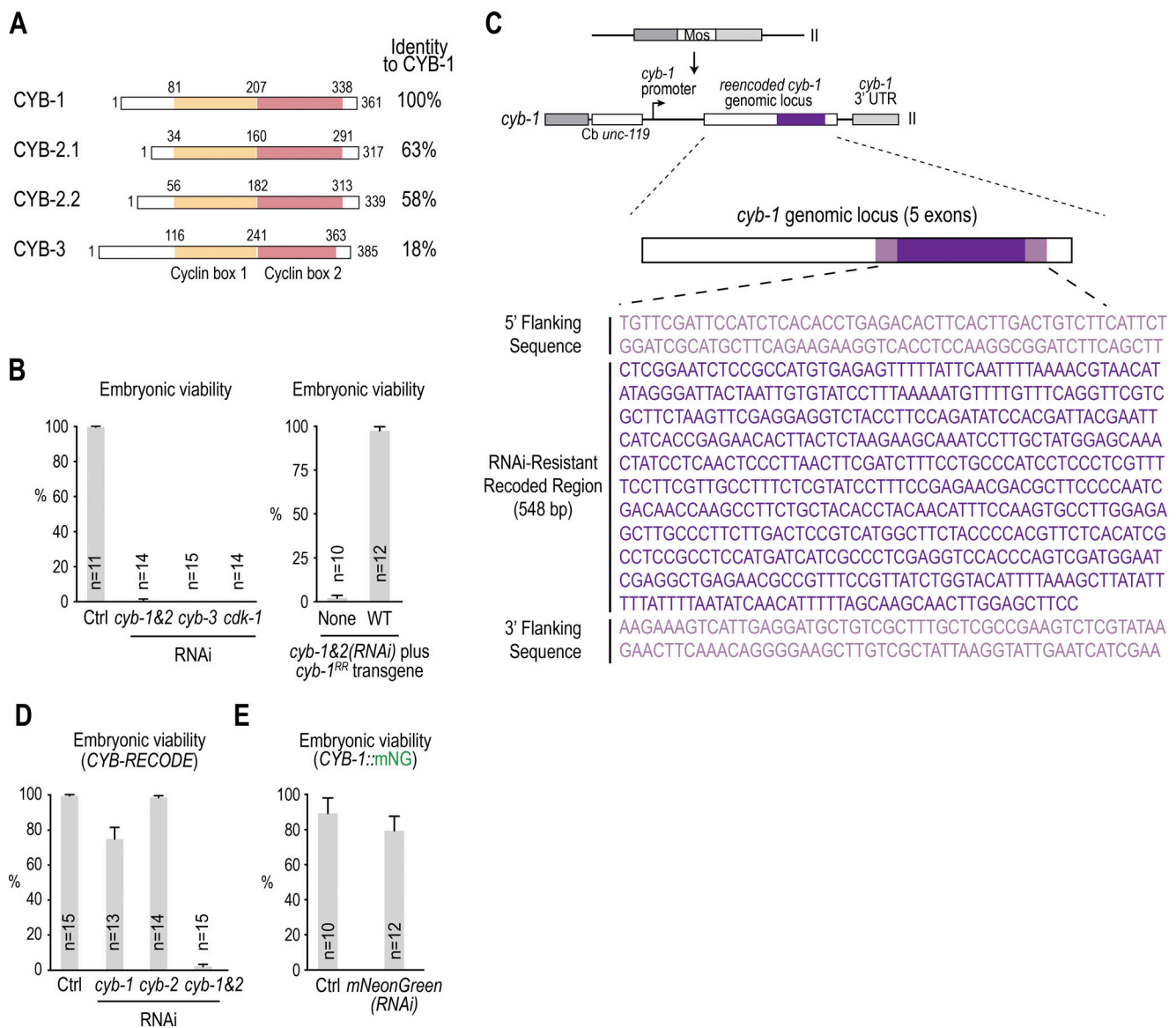


Figure S1. **Validation of the CYB-RECODE system.** (A) Comparison of cyclin B isoforms from *C. elegans*. Numbers indicate amino acid position. (B) Embryonic viability measurements for the indicated conditions. (C) Generation of a *cyb-1* reencoded MosSCI transgene. (D) Embryonic viability measurements for the specified conditions. Note that expression of reencoded *cyb-1* is sufficient to fully rescue the lethality of *cyb-1&2(RNAi)* (B) but *cyb-1* and *cyb-2* are redundantly required to promote embryonic viability (D). (E) Embryonic viability measurements for the specified RNAi conditions in a strain expressing endogenously tagged CYB-1::mNG. Note that individual CYB-1 depletion had a mild effect on embryonic viability (panels D and E), whereas a *cyb-1Δ* mutant is lethal. The reason why the CYB-1 depletion does not exhibit lethality may be because the RNAi conditions for early embryo phenotypic analysis are optimized for depletion of the maternal load; thus, while CYB-1 is largely absent in the early embryonic divisions under these conditions, it is likely synthesized later in embryogenesis following the onset of zygotic gene expression. Error bars are 95% confidence intervals. *n* is the number of adults whose progeny was scored for viability.

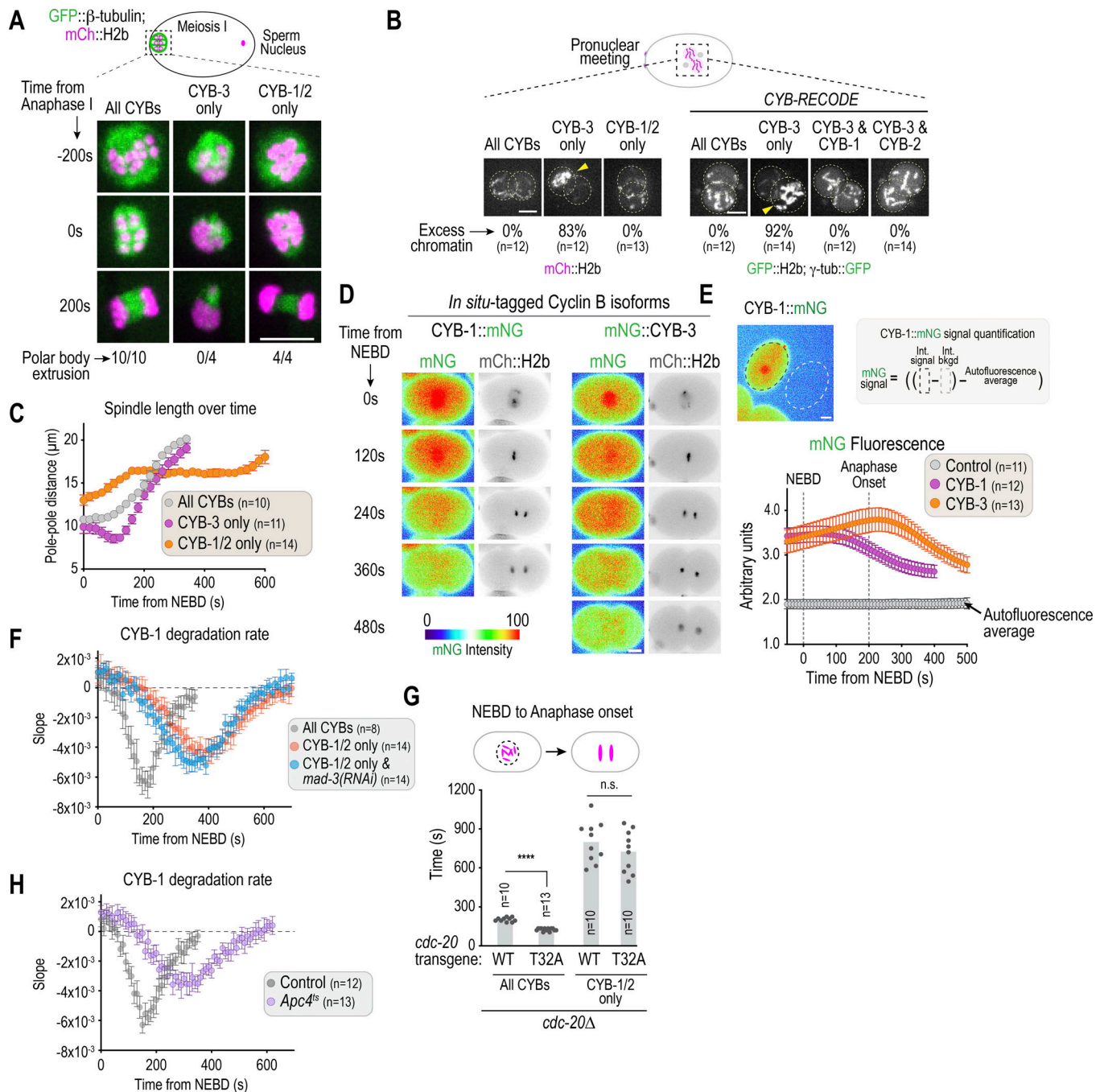


Figure S2. Cyclin B phenotypes in meiosis and spindle elongation and analysis of cyclin B degradation kinetics in mitosis. (A) Time-lapse sequences of embryos undergoing meiosis I under the specified conditions. Quantification of polar body extrusion rates is included below each sequence. We note the presence of defects in spindle assembly and chromosome segregation in CYB-3-only, but not CYB-1/2-only embryos. **(B)** Example images of embryos at pronuclear meeting (75–80 s before NEBD), under the specified conditions. Arrowheads indicate extra chromosomal material signifying meiotic defects (see panel A). Numbers indicate quantification of embryos with excess chromatin for the specified conditions. This analysis indicates that CYB-1 and CYB-2 function redundantly during the meiotic divisions that precede the first embryonic mitosis (van der Voet et al., 2009). **(C)** Measurement of spindle distance over time for the indicated conditions. Whereas CYB-3-only embryos present shortening of the mitotic spindle after NEBD, CYB-1/2 embryos elongate their embryos prematurely (see also Fig. 2 A). **(D)** Example images of embryos expressing in situ-tagged cyclin B isoforms and imaged through time-lapse microscopy. **(E)** Top: Methodology used for the quantification of raw embryonic fluorescence intensity levels. Bottom: Raw fluorescence intensity levels for the specified conditions. The autofluorescence average was calculated in a strain expressing no green fluorophores and was subtracted from the raw values to generate the graphs in Fig. 2, G and H. **(F and H)** Rates of CYB-1 degradation, estimated by measuring the slope of the curves in Fig. 3, E and F, respectively. This analysis revealed that both loss of CYB-3 (F) and direct inhibition of the APC/C through *Apc4^{ts}* (G) similarly delayed the onset of CYB-1 degradation (the point at which the slopes become negative) and reduced the maximum rate of degradation (minimal slope value). **(G)** Quantification of the NEBD-to-anaphase interval in embryos expressing either WT or T32A versions of CDC-20 in a *cdc-20 Δ* background. The “All CYBs” conditions are the same as for Fig. 5 E. Scale bars are 5 μ m (panels A and B) and 10 μ m (panels D and E). Error bars are 95% confidence intervals. *n* is the number of embryos scored per condition. **** represents $P < 0.0001$ from Mann-Whitney tests; non-significant (n.s.) is $P > 0.05$.

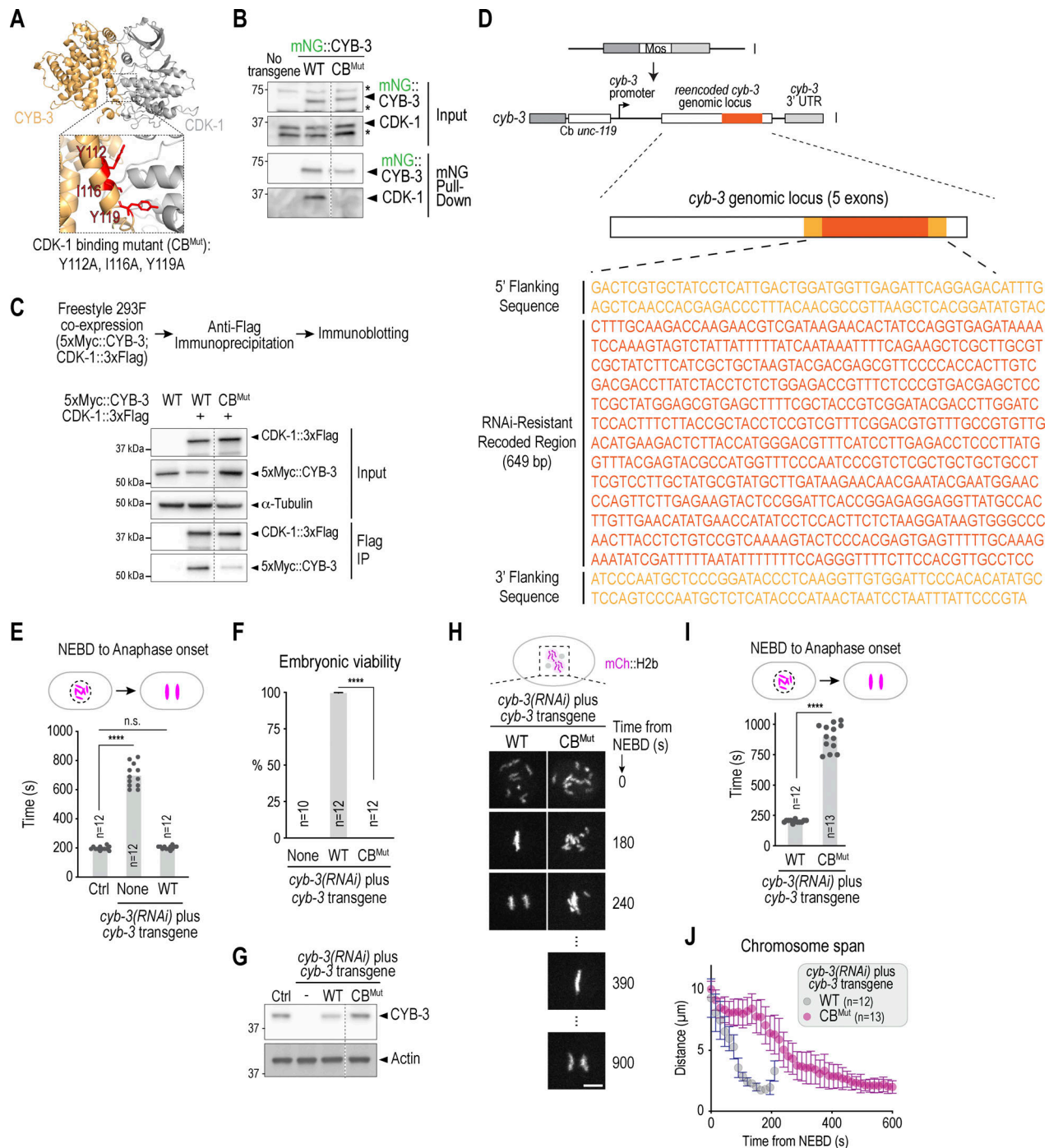


Figure S3. CYB-3 accelerates mitotic events by activating CDK-1. (A) AlphaFold Multimer model of the *C. elegans* CYB-3-CDK-1 complex. Mutated interface residues are shown in red. (B) Immunoblot showing immunoprecipitation of mNG-tagged CYB-3 (WT or CB^{Mut}) from whole worm lysates. Asterisks indicate non-specific bands. (C) Immunoblot of an immunoprecipitation assay used to test the interaction between CDK-1 and CYB-3 mutants expressed in FreeStyle 293-F cells. α -Tubulin is a loading control for the input. (D) Strategy used to generate a *cyb-3* MosSCI transgene that was re-encoded to render it resistant to *cyb-3(RNAi)*. (E) Measurement of mitotic duration in embryos imaged under the specified conditions. The *cyb-3* transgene fully rescues the mitotic duration defect of *cyb-3(RNAi)*. (F) Viability assays for embryos depleted of *cyb-3* by RNAi and expressing the indicated re-encoded *cyb-3* mutants. (G) Immunoblot showing expression of untagged, re-encoded CYB-3 transgenes upon depletion of endogenous CYB-3 by RNAi. Actin is used as a loading control. (H) Example images of embryos expressing mCherry-tagged histone H2b and imaged under the indicated conditions. Scale bar, 5 μ m. (I) Measurement of the NEBD-to-anaphase interval in embryos imaged as in H. Data for WT is the same as in panel E. We note that anaphase onset delay in CB^{Mut} CYB-3 was \sim 200 s longer than CYB-3 depletion (panel E). One potential explanation for the greater severity of CB^{Mut} CYB-3 is that the mutant associates with substrates and competes with CYB-1-CDK-1 complexes that are driving slow mitosis. (J) Measurement of chromosome span for the indicated conditions. Lanes shown in B, C, and G are from a single exposure of the same immunoblot. *n* is the number of adult worms whose progeny were scored (F) or the number of embryos analyzed per condition (E, I, and J). **** represents $P < 0.0001$ from Mann-Whitney tests. Left numbers in B, C, and G represent the positions of the molecular weight marker in kDa. Source data are available for this figure: SourceData FS3.

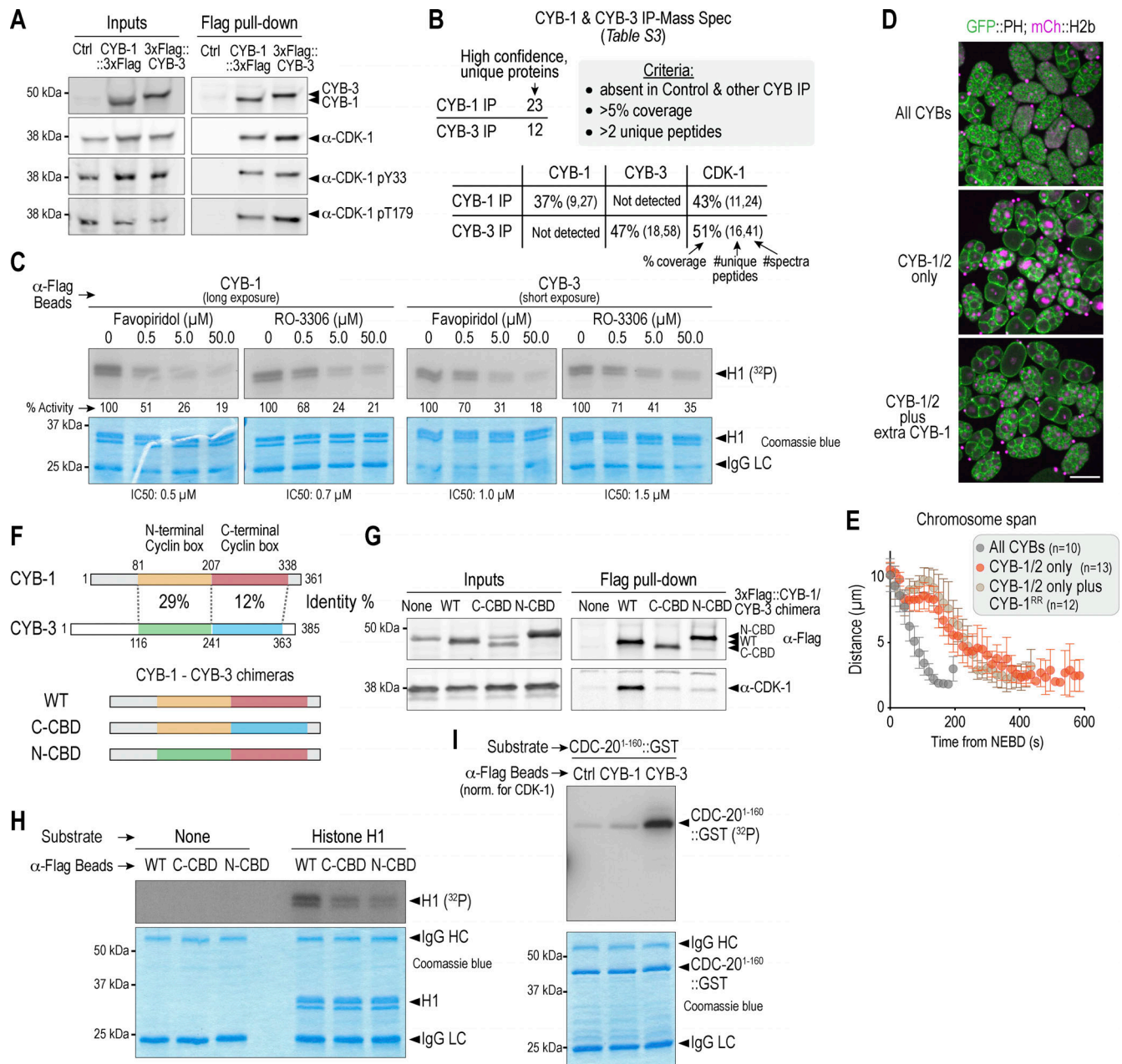


Figure S4. **Biochemical characterization of cyclin B isoforms and analysis of chimeric versions.** (A) Immunoblots showing input extracts and immunoprecipitates of Flag-tagged CYB-1 and CYB-3, as well as co-purified CDK-1. Membranes were also probed for phospho-CDK-1, using antibodies raised against human Cdk1 that recognize the *C. elegans* protein. pY33 corresponds to human pY15 and pT179 corresponds to human pT161. (B) Mass spectrometric analysis of FLAG-tagged CYB-1 and CYB-3 purified from gravid adult extracts; control strain extract was processed in parallel to remove background; the CYB-1 used in this specific analysis was also tagged with mNG. The criteria listed in the gray box were used to identify high-confidence, unique proteins in each immunoprecipitate (IP). The percent coverage, number of unique peptides detected, and total number of spectra are listed below for CYB-1, CYB-3, and CDK-1 in each purification. See Table S3 for the full list of hits, which were defined as proteins with at least two unique peptides and that were not identified in the control pull-down sample (see Materials and methods). (C) In vitro kinase assays using Flag-tagged CYB proteins immunoprecipitated from embryo extracts, in the presence or absence of the CDK-1 inhibitors Flavopiridol and RO-3306. Numbers under each exposure indicate remaining activity relative to untreated controls and were used to estimate IC50s for each inhibitor (see Materials and methods). Note that CYB-1 assays were exposed for longer to obtain a comparable signal to CYB-3 assays. IgG LC corresponds to the Ig light chain. (D) Snapshot of developing embryos expressing mCherry-histone and a GFP-tagged plasma membrane marker. Note that, compared to controls, embryos expressing CYB-1/2 only contain nuclei with high levels of mCherry-Histone, likely arising from endoreplication. This phenotype is suppressed by the addition of extra CYB-1. Scale bar, 40 μm. (E) Quantification of the chromosome span for the conditions in Fig. 4 F. (F) Top: Schematic comparing the sequences of CYB-1 and CYB-3, highlighting the N-terminal cyclin box (N-CBD) and C-terminal cyclin box (C-CBD). Bottom: Schematic illustrating the chimeras used in this study. (G) Immunoblots showing input extracts and immunoprecipitates of Flag-tagged CYB-1 WT or chimeras (N-CBD, C-CBD), as well as co-purified CDK-1. (H and I) In vitro kinase assays using Flag-tagged CYB proteins immunoprecipitated from embryo extracts and using either histone H1 (H) or CDC-20¹⁻¹⁶⁰::GST (I) as a substrate. IgG HC and IgG LC correspond to the Ig heavy and light chains, respectively. Note that cyclin B-CDK-1 complexes do not phosphorylate GST alone (Fig. 4 D). Left numbers in A, C, G, H, and I represent the positions of the molecular weight marker in kDa. Source data are available for this figure: SourceData FS4.

Provided online are three tables. Table S1 lists the strains used in this study. Table S2 shows oligonucleotides used for dsRNA production. Table S3 shows mass spectrometry analysis of CYB-1 and CYB-3 interactors.